General Disclaimer

One or more of the Following Statements may affect this Document

- This document has been reproduced from the best copy furnished by the organizational source. It is being released in the interest of making available as much information as possible.

- This document may contain data, which exceeds the sheet parameters. It was furnished in this condition by the organizational source and is the best copy available.

- This document may contain tone-on-tone or color graphs, charts and/or pictures, which have been reproduced in black and white.

- This document is paginated as submitted by the original source.

- Portions of this document are not fully legible due to the historical nature of some of the material. However, it is the best reproduction available from the original submission.

NASA CR-134974

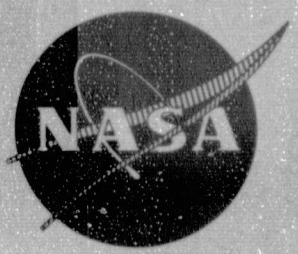

STRAINRANGE PARTITIONING BEHAVIOR OF AN AUTOMOTIVE TURBINE ALLOY

FINAL REPORT

by C. G. Annis, M. C. VanWanderham, and R. M. Wallace

PRATT & WHITNEY AIRCRAFT

FLORIDA RESEARCH AND DEVELOPMENT CENTER

Prepared For

NATIONAL AERONAUTICS AND SPACE ADMINISTRATION

NASA Lewis Research Center

Contract NAS3-18930

1. Report No.	2. Government Accession No.	3. Recipient's Catalog No.
NASA CR-134974		

4. Title and Subtitle	5. Report Date
Strainrange Partitioning Behavior of an Automotive Turbine Alloy	February 1976
	6. Performing Organization Code

7. Author(s)	8. Performing Organization Report No.
C. G. Annis, M. C. VanWanderham, R. M. Wallace	FR-7424
	10. Work Unit No.

9. Performing Organization Name and Address	11. Contract or Grant No.
Pratt & Whitney Aircraft Florida Research and Development Center West Palm Beach, Florida	NAS3-18930
	13. Type of Report and Period Covered Final Contractor Report - 13 Dec 1974 through 13 Dec 1975

12. Sponsoring Agency Name and Address	14. Sponsoring Agency Code
Energy Research and Development Administration Washington, D. C. 20545	

15. Supplementary Notes

Project Manager, Dr. Gary R. Halford, NASA Lewis Research Center, Cleveland, Ohio

16. Abstract

This report addresses Strainrange Partitioning, an advanced life prediction analysis procedure, as applied to CA-101 (cast IN 792 + Hf), an alloy proposed for turbine disks in automotive gas turbine engines. The methodology was successful in predicting specimen life under thermal-mechanical cycling, to within a factor of ±2. This work was funded by the Office of Highway Vehicle Systems, Office of Conservation, Energy Research and Development Administration.

17. Key Works (Suggested by Author(s))	18. Distribution Statement
Strainrange Partitioning CA-101 IN-792 + Hf life prediction thermal mechanical testing low-cycle fatigue	Unclassified, unlimited

19. Security Classif. (of this report)	20. Security Classif. (of this page)	21. No. of Pages	22. Price *
Unclassified		79	$3.00

*For sale by the National Technical Information Service, Springfield, Virginia 22151

CONTENTS

SECTION I
SUMMARY

Contract NAS3-18930 investigated the low-cycle fatigue (LCF) resistance of CA-101 (Cast IN 792 + Hf), an alloy proposed for automotive turbine disks, using Strainrange Partitioning.

Strainrange Partitioning, an advanced life prediction analysis procedure, assumes that any hysteresis loop can be represented by combinations of the four generic cycle definitions: PP, PC, CP, and CC. The first letter refers to the material response in tension, either Plastic (strain which is not time dependent) or Creep (time dependent strain), and the second letter refers to material response in compression.

To quantify the LCF behavior of CA-101, axially strain controlled tests of each of the four generic types were performed at three elevated temperatures, 538°C, 760°C, and 927°C (1000°F, 1400°F, and 1700°F). These results were then used to predict specimen life under thermal-mechanical strain cycling (TMSC), using the Strainrange Partitioning methodology.

Results were encouraging: TMSC predictions were accurate to within a factor of ±2, the same data scatter observed in the basic isothermal LCF tests.

SECTION II
INTRODUCTION

A. RELATIONSHIP TO AUTOMOTIVE GAS TURBINE ENGINE

This program investigates the high temperature, strain-cycling fatigue resistance of CA-101 (Cast IN 792 + Hf), an alloy proposed for turbine disks in automotive gas turbine engines. The Federal Government and private corporations have placed considerable emphasis on the development of automotive gas turbine engines that offer low exhaust emissions and high potential fuel economies. To be cost effective, long operating life is also required.

Experience with gas turbine engine disks has indicated that low-cycle fatigue (LCF) is often the life-limiting factor. Accurate LCF life predictions are based on a thorough understanding of the response of the material during complex thermal-mechanical strain cycling. The advanced analysis procedure, Strainrange Partitioning, is ideally suited to this purpose.

B. GENERAL EXPLANATION OF STRAINRANGE PARTITIONING

Strainrange Partitioning (SRP) is a life prediction analysis procedure for high temperature, low-cycle fatigue involving creep-fatigue interactions. The procedure addresses material behavior under cyclic deformation, paying particular attention to inelastic strain-time synergism.

The inelastic strains are divided into those which are time-dependent, and those which are not. For convenience, time-dependent inelastic strain is termed "creep," and time-independent inelastic strain "plastic." Since these strains can be experienced in both tension and compression, four combinations of inelastic strain are possible: (1) plastic in both tension and compression, PP, (2) plastic in tension, creep in compression, PC, (3) creep in tension, plastic in compression, CP, and finally (4) creep in both tension and compression CC. The continued development of this procedure into a life prediction methodology suitable for accurately calculating cyclic life under some thermal-mechanical cycle, is the topic of this report.

SECTION III
THE ALLOY, CA-101, METALLURGICAL DESCRIPTION AND BASIC MECHANICAL PROPERTIES

A. METALLURGICAL DESCRIPTION, COMPOSITION, HEAT TREATMENT

The alloy investigated in this program was the cast, nickel-base superalloy, CA-101 (Hafnium modified IN-792). The alloy was cast from Heat 140E3429, the same master heat used by Austenal-Dover Division of Howmet for integrally-bladed turbine disks, and arrived in the form of cast test bars 16-mm (5/8 in.) diameter by 100-mm (4 in.) long. The chemical composition is given in table I.

Table I. Chemical Composition of CA-101

Element	Range by Weight, %			
Carbon	0.11	to	0.16	
Chromium	12.0	to	13.0	
Cobalt	8.5	to	9.5	
Molybdenum	1.7	to	2.2	
Tungsten	3.8	to	4.2	
Tantalum	3.8	to	4.2	
Titanium	3.9	to	4.2	Ti+Al 7.3 to 7.7
Aluminum	3.3	to	3.7	
Hafnium	0.8	to	1.2	
Boron	0.01	to	0.02	
Zirconium	0.1	to	0.15	
Manganese	0.1	Maximum		
Silicon	0.1	Maximum		
Phosphorus	0.015	Maximum		
Sulfur	0.015	Maximum		
Iron	0.5	Maximum		
Nickel	Balance			

The test bars were heat treated to the same specification applied to cast integral turbine disks:

1. Heated at 1121°C (2050°F) for 2 hr in vacuum; cooled at a rate equivalent to air cool.

2. Heated at 843°C (1550°F) for 24 hr in argon; air cooled.

Cross-sectional views of the macrostructure of the test bars before and after heat-treatment are shown in figure 1. The cast test bars show relatively coarse grain size, average grain size of 6 to 10 mm (1/4 to 3/8 in.). Fine columnar grains initiated at the bottom surface with coarser grains through the balance of the bar, growing transversely across the gage length of the bar from the outer diameter and meeting approximately along the centerline of the bar. A small amount of shrinkage and porosity was evident.

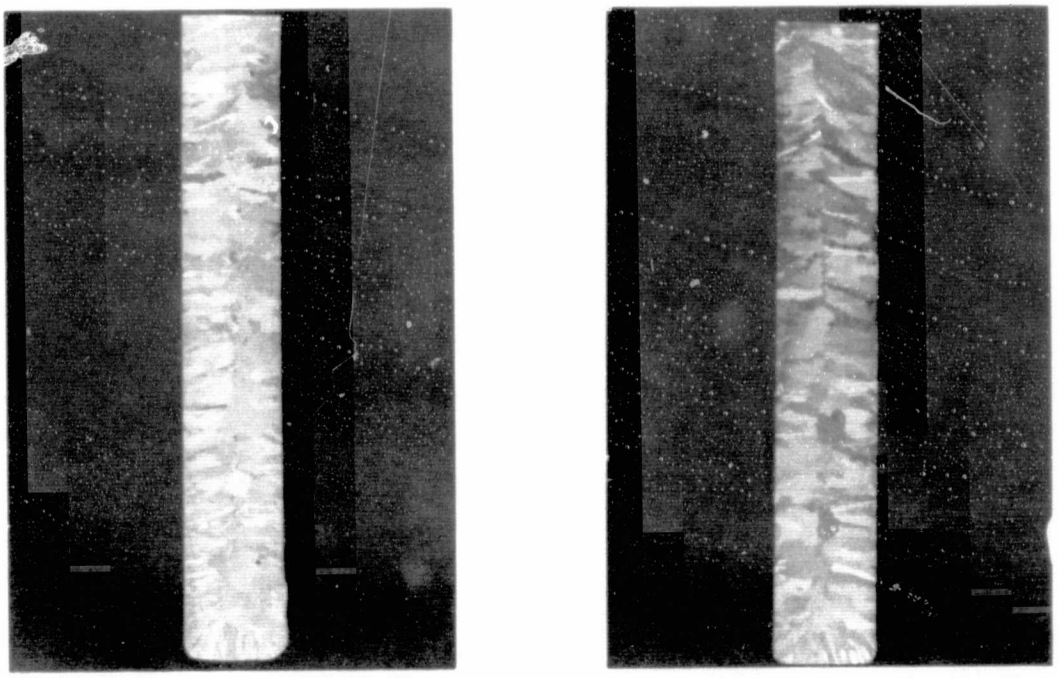

FAL 34616 FAL34636

As-Cast Heatreated

Figure 1. Cross-Section of CA101 Cast Test Bars FD 87471

B. TENSILE AND CREEP PROPERTIES

Five creep tests, at 760°C (1400°F), and eight tensile tests at four temperatures, room temperature, 538°C, 760°C, and 927°C (1000°F, 1400°F, 1700°F) determined the mechanical properties of CA-101. Tensile properties, including ultimate tensile strength, yield strength (0.02% and 0.2% offset), percent reduction of area, strain hardening exponent, and true fracture strength, were obtained for each of the specimens tested. Plots of strength and ductility vs temperature are provided in figure 2.

Table II presents the tensile properties of CA-101, creep properties are given by table III.

C. DISCUSSION - MECHANICAL PROPERTIES OF THIS HEAT

Strength and ductility of this material are lower than expected. Table IV compares the room temperature properties of the CA-101 being investigated in this program and published results of CA-101, (Reference: MCIC Report/ September 1972, "Superalloys . . . Processing" pages BB 11-12). This comparison with a single source is not sufficient to conclude that a problem with the material exists. The CA-101 cast test bars received meet the defined requirements (size, chemical composition, radiographically sound, and heat treatment); therefore, the source of strength discrepancy may lie in the casting procedure.

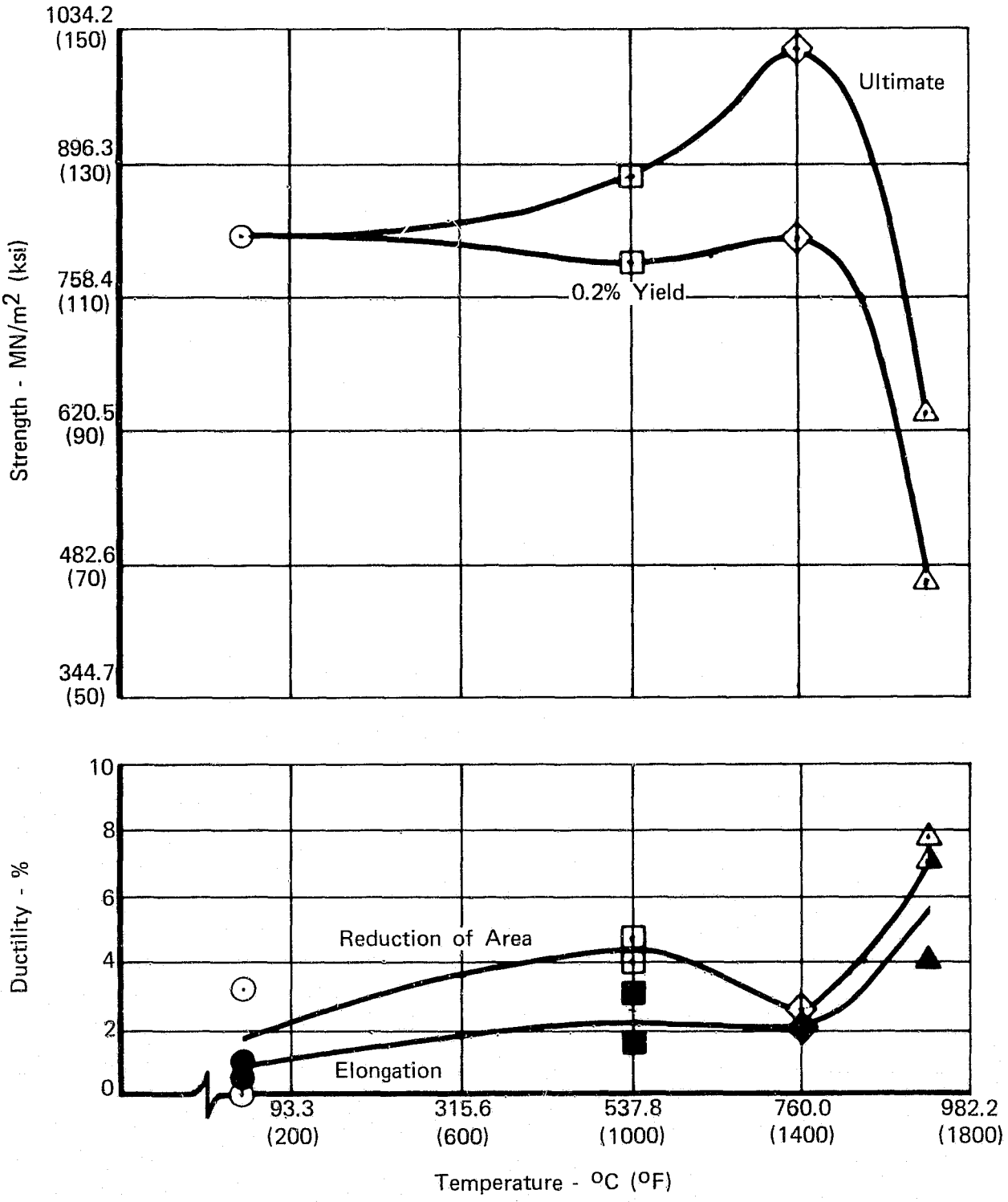

Figure 2. Strength and Ductility vs Temperature for CA101 FD 97727

Table II. Tensile Properties of CA-101

Specimen Identity	Test Temperature °C	Test Temperature °F	Strength (Engineering) Yield 0.02% Offset MN/m²	Yield 0.02% Offset ksi	Yield 0.2% Offset MN/m²	Yield 0.2% Offset ksi	Ultimate True Fracture MN/m²	Ultimate True Fracture ksi	Ultimate Engineering MN/m²	Ultimate Engineering ksi	Ductility EL, %	Ductility RA, %	Modulus of Elasticity, psi x 10^6	Poisson's Ratio	Strain Hardening Exponent, n
T2	RT	RT	780.5	113.2	828.7	120.2	833.6	120.9	828.7	120.2	1.0	3.2	26.7	0.36	(1)
T5	RT	RT	707.4	102.6	816.3	118.1	820.5	119.0	816.3	118.4	0.5	negligible	27.2	0.30	(1)
T1	538	1000	681.0	99.2	795.0	115.3	901.0	130.7	887.4	128.7	1.5	4.0	25.9		0.16
T6	538	1000	674.3	97.8	790.8	114.7	890.1	129.1	876.3	127.1	3.0	4.7	25.4		0.13
T3	760	1400	716.4	103.9	817.0	118.5	1027.3	119.0	1008.0	146.2	2.0	2.4	20.2		0.30
T7	760	1400	626.0	90.8	835.6	121.2	983.9	142.7	970.1	140.7	2.0	2.0	22.3		0.22
T4	927	1700	350.9	50.9	171.6	68.4	607.4	88.1	637.8	92.5	4.0	7.1	15.6		0.02
T8	927	1700	339.9	49.3	467.5	67.8	614.3	89.1	635.0	92.1	7.0	7.9	19.8		(2)

(1) Test displayed limited ductility, strain hardening exponent not obtainable.

(2) Specimen necked immediately after yield.

Table III. Creep and Creep Rupture Properties of CA-101

Specimen Identity	Temperature °C	Temperature °F	Stress Level MN/m²	Stress Level ksi	Time to 1% Creep Strain, hr	Onset of 3rd-Stage Creep, hr	Rupture, hr	Elongation at Failure, %	Reduction of Area at Failure, %
C2	760	1400	482.6	70	267.0	223.0	267.0	1.06	1.0
C4	760	1400	517.1	75	299.0	360.0	579.0	3.0	8.5
C3	760	1400	551.6	80	200.0	230.0	300.0	2.27	4.4
C5	760	1400	586.1	85	65.0	85.0	90.0	1.6	4.4
C1	760	1400	620.5	90	27.2	28.6	35.0	1.8	2.8

Table IV. Comparison of CA-101 Properties at Room Temperature

	CA-101 Program Test T2	Test T5	CA-101 Literature
Ultimate Tensile Strength	120 ksi	118 ksi	170 ksi
0.2% Yield Strength	120 ksi	118 ksi	145 ksi
Elongation	1%	0.5%	7%
Reduction of Area	3.2%	≈0%	9%

SECTION IV
GENERATION OF BASIC STRAINRANGE PARTITIONING RELATIONSHIPS

A. STRAINRANGE PARTITIONING OVERVIEW

Strainrange Partitioning is a life prediction analysis procedure for high temperature, low-cycle fatigue involving creep-fatigue interactions, which addresses material behavior under cyclic deformation (hysteresis), paying particular attention to inelastic strain-time synergism.

The inelastic strains are divided into those which are time-dependent, and those which are not. For convenience, time-dependent inelastic strain is termed "creep," and time-independent inelastic strain "plastic." Since these strains can be experienced in both tension and compression, four combinations of inelastic strain are possible: (1) plastic in both tension and compression, PP, (2) plastic in tension, creep in compression, PC, (3) creep in tension, plastic in compression, CP, and (4) creep in both tension and compression, CC.

Any hysteresis loop can be described as some combination of these elements, each present in amounts represented by their constitutive fractions, $F_{a,b}$. The first literal subscript refers to the type of inelastic strain experienced in tension, the second subscript refers to that in compression. Only three, of the four basic types, of inelastic strainrange can be present in any real hysteresis loop. Both PP and CC can occur together in a cycle but only one PC or CP type can be present. This is because with PC or CP there is creep in only one-half of the cycle being reversed by plastic deformation. Since it is physically possible to have "more" creep in only one-half of any real hysteresis loop, only one, PC or CP type can be present.

When the constitutive fractions have been determined (Section V.B) the expected cyclic life can be calculated from The Interaction Damage Rule:

$$1/N_f = F_{pp}/N_{pp} + F_{pc}/N_{pc} + F_{cp}/N_{cp} + F_{cc}/N_{cc}$$

where:

N_f = cyclic life under some complex hysteresis loop

$F_{a,b}$ = constitutive fraction of type a,b inelastic strain contained in that hysteresis loop

and:

$N_{a,b}$ = cyclic life expected were the entire inelastic strain of type a,b. (Section V.C.)

The following subsections examine, in detail, the basic tests and their analyses. Section IV addresses the application of these LCF results to life prediction.

B. BASIC LOW-CYCLE FATIGUE TESTS

A series of four basic types of low-cycle fatigue tests were performed on the alloy CA-101. Three temperatures were chosen that represent the operating range of an integrally-bladed turbine disk in an automotive gas turbine engine, 538°C, 760°C, and 927°C (1000°F, 1400°F, and 1700°F).

The four types of axially-loaded, strain-controlled, low-cycle fatigue tests are:

1. PP - High-frequency (1.0 Hz), completely reversed, strain-controlled fatigue tests using a triangular, axial strain vs time waveform.

2. CC - Tensile and compressive strain hold-time test in which a hold period of 2 or 5 min was applied while at both the peak axial tensile and compressive strains of the cycle. The remainder of the cycle was applied under completely reversed axial strain-control at a cyclic frequency of 1.0-Hz using a triangular strain vs time waveform.

3. CP - Tensile strain hold-time test in which a hold period of 2 or 5 min was applied while at the peak axial tensile strain of the cycle. The remainder of the cycle was applied under completely reversed, axial strain-control at a cyclic frequency of 1.0 Hz using a triangular strain vs time waveform.

4. PC - Compressive strain hold-time test in which a hold period of 2 or 5 min was applied while at the peak compressive axial strain of the cycle. The remainder of the cycle was applied under completely reversed, axial strain-control at a cyclic frequency of 1.0-Hz using a triangular strain vs time waveform. These strain-time cycles are illustrated in figure 3. Figure 4 depicts the stress-strain relationships.

C. DESCRIPTION OF TEST EQUIPMENT AND SPECIMEN

Axial-strain, low-cycle fatigue characteristics were determined at various temperatures, strain rates, and strain waveforms on servohydraulic, closed-loop, fatigue testing machines, designed and built at the Pratt & Whitney Aircraft (P&WA), Florida Research and Development Center (FRDC). (See figure 5.)

The specimen that was used is shown in figure 6. Four basic requirements guided specimen design and development. These were:

1. Strain distribution be known over the gage section

2. Axial strain be accurately measurable

3. There be minimum strain concentrations

4. Failure location be in the gage section.

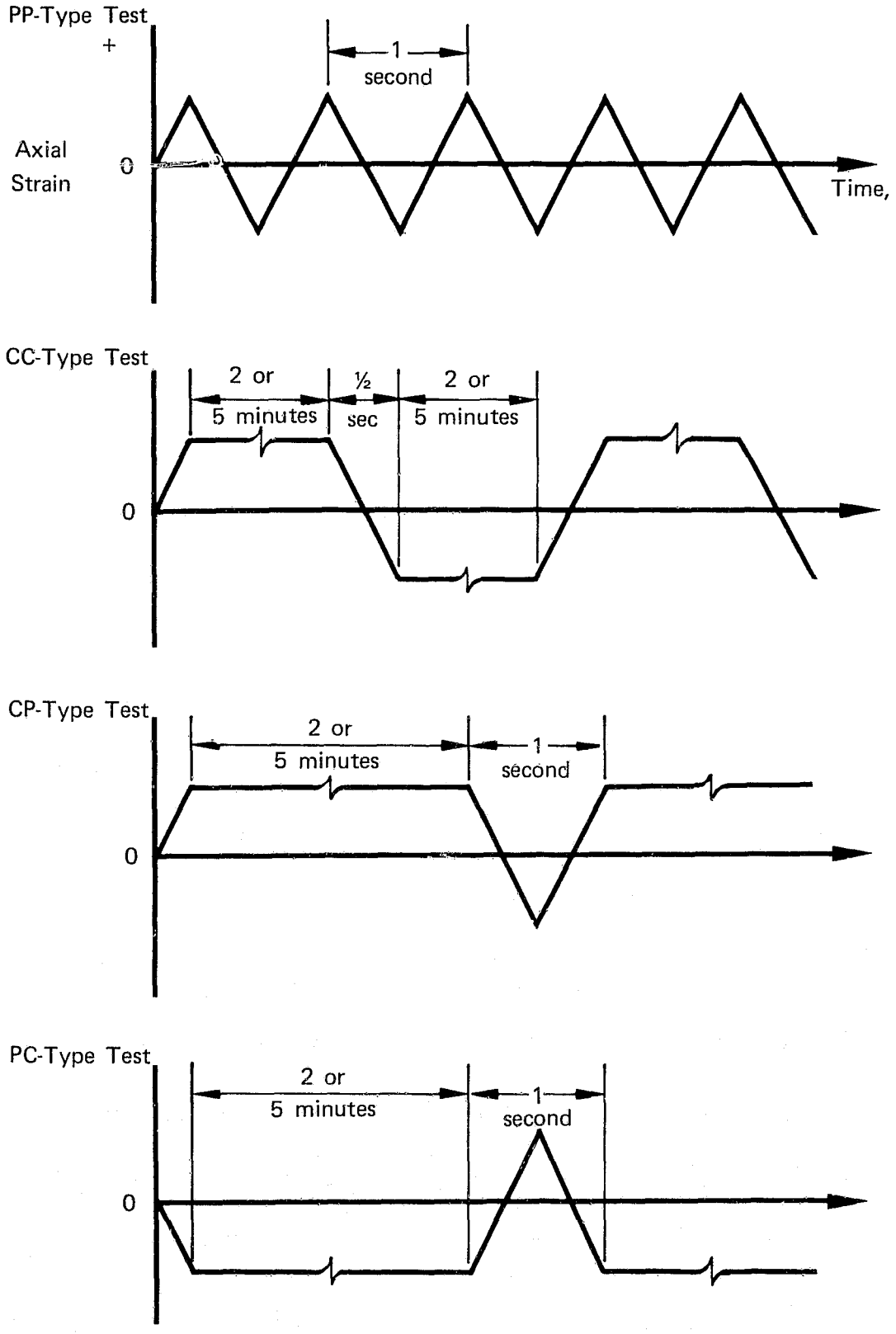

Figure 3. Axial Strain vs Time Waveforms for the Isothermal Low-Cycle Fatigue Tests FD 95912

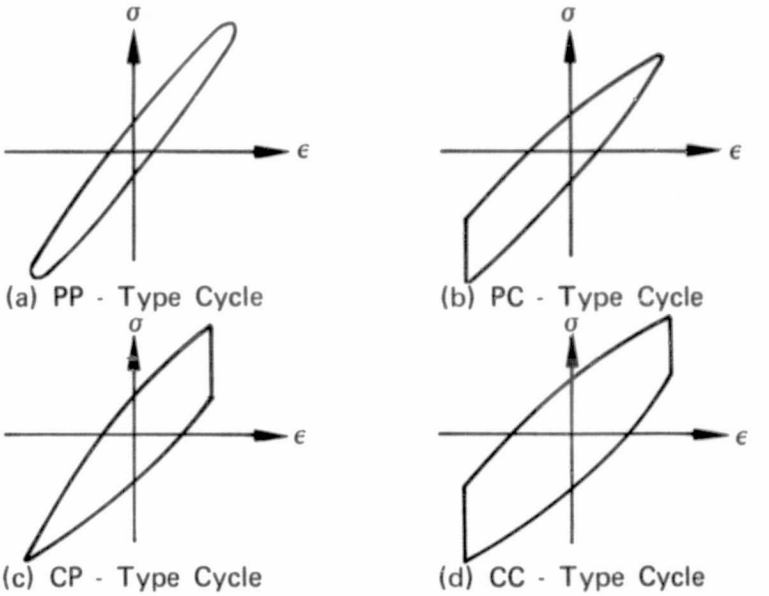

Figure 4. Idealized Stress-Strain Representations of the Four Basic Cycle Types FD 95913

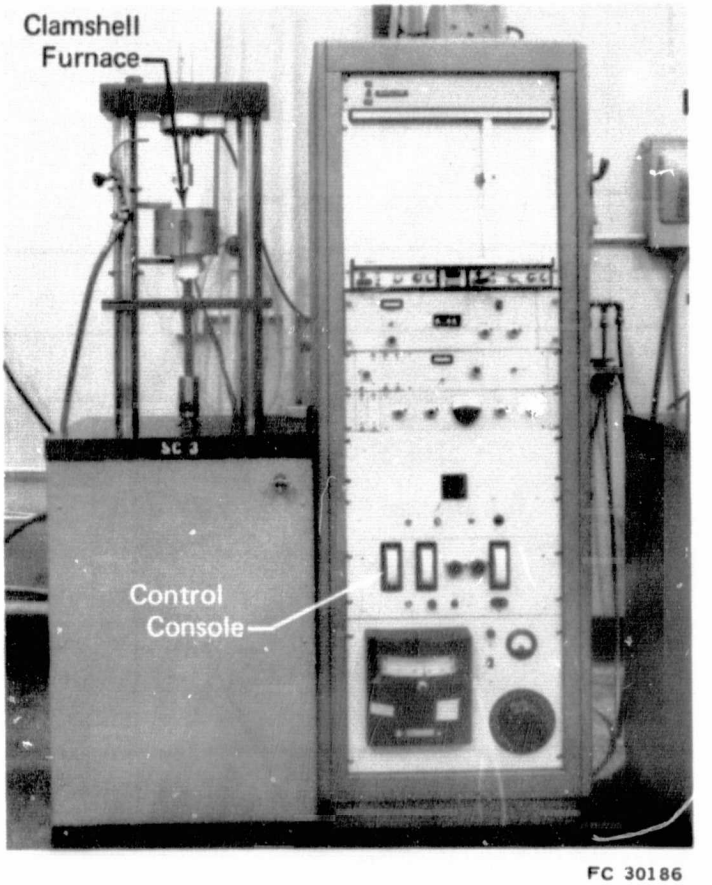

Figure 5. Servohydraulic, Closed-Loop, Low-Cycle Fatigue Testing Machine Controlled by Command Signal from a Digital-to-Analog Function Generator FD 95914

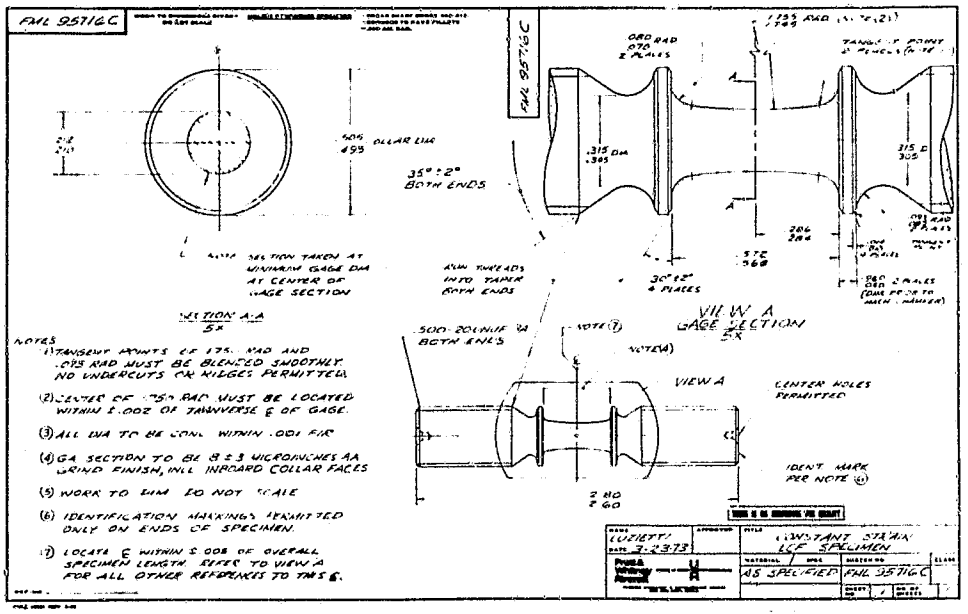

Figure 6. Constant Strain LCF Specimen FML 95716C

Additional requirements were that the specimen lend itself easily to installation, and that calculations necessary for establishing machine operating parameters be simple.

The final specimen configuration, which incorporated integral machined extensometer collars, was determined experimentally using photoelastic and elastic-plastic strain analyses. A calibration procedure was established to relate the maximum strain to collar deflection during both the elastic and the plastic portions of the strain cycle. The plasticity correction accounts for the possible deviation of apparent (extensometer) strain, $\Delta\ell/\ell$, from the true strain.

Strain is defined as the ratio of increased length, $\Delta\ell$, to an original length, ℓ. In the elastic region, any increase in length occurs over the entire gauge length but plastic deformation occurs locally. The plasticity correction, corrects for the change in effective gage length with the onset of plasticity. The extensometer deflection always accurately records $\Delta\ell$.

Fortunately, a simple method to correct for this has been devised[1]. A thorough finite element analysis of the FRDC strain control specimen showed that the plasticity correction factor, C_1/C_2, is uniquely related to material strain hardening exponent, n. Since the computation of n is straightforward, given the material cyclic stress-strain curve, the correction factor is also easily computed.

---

[1] deNeeve, P. F., and A. Wuerscher, "Evaluation of the Strain Behavior of an LCF Specimen Developed by FRDC," Internal Report, United Aircraft of Canada, Ltd.

Specimen axial strain was measured and controlled by means of a proximity probe extensometer. Collar deflection was measured and controlled via proximity probes attached to the open ends of the extensometer tubes so that the extensometer rod ends move relative to the probes as the specimen collars deflect, as shown in figure 7.

Load measurement was accomplished by a commercial tension-compression load cell.

An x-y recorder was used for recording load vs strain plots at predetermined cyclic intervals during testing. Prior to each test the x-y recorder was calibrated with the extensometer at the prescribed test temperature so that the ratio of specimen collar deflection to x-y recorder pen movement in "x" direction was known. The "y" axis of the x-y recorder calibrated with the load cell so that the ratio of specimen load to x-y recorder pen movement was known. Load calibration was the same for both room and elevated temperature tests (figure 8).

To obtain good resolution of the hysteresis characteristics at frequencies near or above the response limits of the x-y recorder, an oscillograph was used. The simultaneously generated plots of strain vs time and load vs time could then be used to provide the required strain vs load hysteresis plot.

The command signal for the strain cycle was produced by a triangular wave signal generator with feedback from the extensometer output to complete the closed-loop-on-strain circuit necessary for the triangular strain waveform. The frequency and ramp of the triangular wave, and, therefore, the strain rate could be adjusted from 0.3×10^{-6} to $0.2\ sec^{-1}$.

An adjustable timing circuit in the cycle control unit of the low-cycle fatigue testing machine was used to maintain dwell at the maximum and minimum strain required. The specimen was strained at the rate set by the signal generator until the required maximum strain limit was attained. At this point, the signal generator was switched out of the circuit, and a timed "sense and hold" sequence then maintained the strain limit for the prescribed time period. Then the signal generator was switched back into the circuit to decrease the strain at the proper strain rate to the lower limit. When the lower limit set-point was reached, the command signal reversed direction and cycle was repeated. This sequence was completely reversed to obtain a dwell at the lower limit or combined to obtain a dwell at both the upper and lower limits.

A memory oscilloscope was used and photographs obtained periodically to monitor strain vs time output to verify conformance to the wave input form.

The specimens were cycled to failure with load-strain plots being obtained at cyclic intervals throughout the life of the specimen. The accumulated number of cycles to each load strain plot and the total number of cycles to complete specimen failure were recorded.

D. PRESENTATION AND DISCUSSION OF BASIC LCF TEST RESULTS

A minimum of 14 tests were performed for each of the four basic low-cycle fatigue tests (PP, CC, PC, CP). A minimum of six of the basic tests were conducted at the intermediate temperature, 760°C (1400°F), and four tests were conducted for each basic type at each of two different temperatures, 538°C (1000°F), and 927°C (1700°F). Test conditions and results of all basic LCF tests are presented in table V.

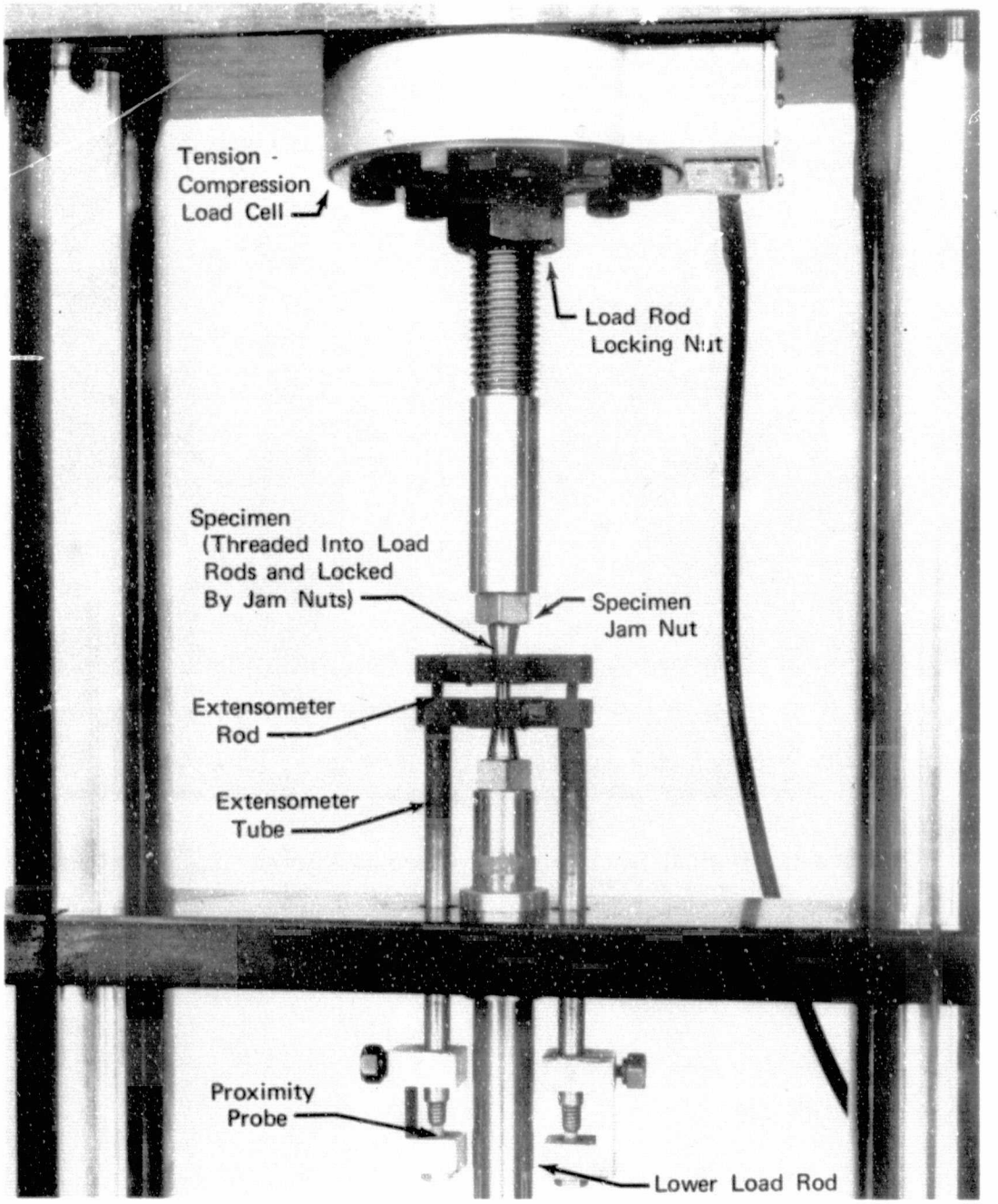

Figure 7. Load Cell, Load Rod, Specimen, and Extensometer Assembly Mounted in Low-Cycle Fatigue Machine FD 92637

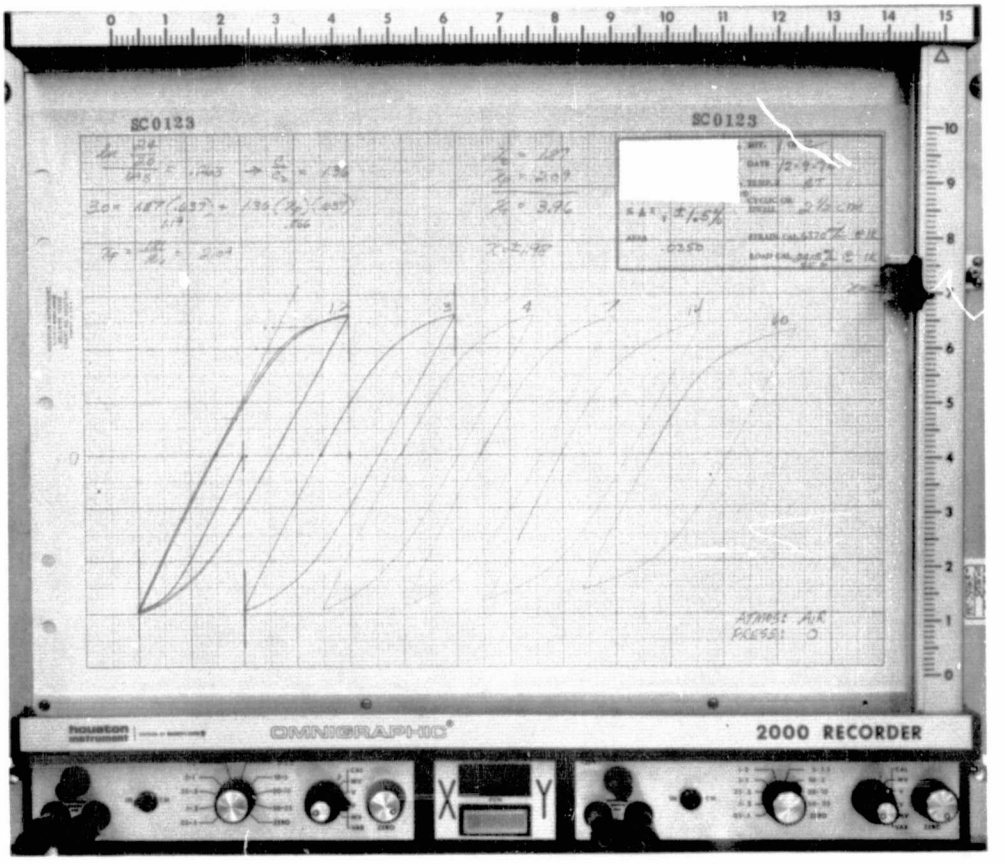

Figure 8. Typical Load-Strain Hysteresis Curves Recorded During a Strain-Controlled Low-Cycle Fatigue Test FD 72642

Table V. Basic Low-Cycle Fatigue Tests

Specimen Identity	Test Temperature °C	Test Temperature °F	Cycle Defintion	Total Strain Amplitude	Inelastic Strainrange, μ in./in.	Cycles to Failure
PP-1A	538	1000	1.0 Hz	±0.00500	63	1,500
PP-2	760	1400	1.0 Hz	±0.00352	16	66,000
PP-3	538	1000	1.0 Hz	±0.00456	37	3,700
PP-4	538	1000	1.0 Hz	±0.00405	13	16,687
PP-5	760	1400	1.0 Hz	±0.00500	200	323
PP-6	760	1400	1.0 Hz	±0.00402	45	7,225
PP-7	760	1400	1.0 Hz	±0.00406	35	5,595
PP-8	760	1400	1.0 Hz	±0.00377	30	1,650
PP-9	760	1400	1.0 Hz	±0.00375	25	4,100
PP-10	538	1000	1.0 Hz	±0.00556	258	240
PP-11	927	1700	1.0 Hz	±0.00252	48	11,700
PP-12	927	1700	1.0 Hz	±0.00303	125	4,130
PP-13	927	1700	1.0 Hz	±0.00335	113	4,950
PP-14	927	1700	1.0 Hz	±0.00375	165	2,180
CP-15	538	1000	2 min - T dwell	±0.00517	225	545
CP-16	538	1000	2 min - T dwell	±0.00464	175	650
CP-17	538	1000	5 min - T dwell	±0.00618	750	53
CP-18	538	1000	2 min - T dwell	±0.00400	125	7,991
PP-19	760	1400	1.0 Hz	±0.00671	1125	46
CP-19B	760	1400	2 min - T dwell	±0.00650	850	342
CP-20	760	1400	2 min - T dwell	±0.00500	225	1,736
CP-20B	760	1400	2 min - T dwell	±0.00678	1025	123
CP-21	760	1400	2 min - T dwell	±0.00600	650	362
CP-22	760	1400	2 min - T dwell	±0.00400	225	3,783
CP-23	760	1400	5 min - T dwell	±0.00500	400	1,679
CP-24	760	1400	5 min - T dwell	±0.00590	900	513
CP-25	927	1700	2 min - T dwell	±0.00350	1050	1,100
CP-25A	927	1700	2 min - T dwell	±0.00425	1287	135
CP-25B	927	1700	5 min - T dwell	±0.00450	2000	245
CP-26	927	1700	2 min - T dwell	±0.00410	950	945
CP-27	927	1700	2 min - T dwell	±0.00337	900	961
CP-28	927	1700	5 min - T dwell	±0.00250	250	2,268 (Failed Prematurely)
PC-29	538	1000	2 min - C dwell	±0.00500	225	514
PC-30	538	1000	5 min - C dwell	±0.00450	100	3,158
PC-31	538	1000	2 min - C dwell	±0.00520	135	772
PC-32	538	1000	2 min - C dwell	±0.00560	675	191

Table V. Basic Low-Cycle Fatigue Tests (Continued)

Specimen Identity	Test Temperature °C	°F	Cycle Definition	Total Strain Amplitude	Inelastic Strainrange, μin./in.	Cycles to Failure
PC-33	760	1400	2 min - C dwell	±0.00600	875	45
PC-34	760	1400	2 min - C dwell	±0.00346	65	1,632
PC-35	760	1400	2 min - C dwell	±0.00493	430	245
PC-36	760	1400	2 min - C dwell	±0.00390	75	1,546
PC-37	760	1400	5 min - C dwell	±0.00450	125	225
PC-38	760	1400	5 min - C dwell	±0.00550	620	205
PC-39	927	1700	2 min - C dwell	±0.00300	275	310
PC-40	927	1700	5 min - C dwell	±0.00245	135	554
PC-41	927	1700	2 min - C dwell	±0.00200	275	800
PC-42	927	1700	2 min - C dwell	±0.00334	730	134
CC-43	538	1000	2 min - T, C dwell	±0.00560	225	240
CC-44	538	1000	2 min - T, C dwell	±0.00460	200	998
CC-45	538	1000	2 min - T, C dwell	±0.00600	1250	44
CC-46	538	1000	2 min - T, C dwell	±0.00410	125	1,342
CC-47	760	1400	2 min - T, C dwell	±0.00490	1100	503
CC-48	760	1400	2 min - T, C dwell	±0.00600	2500	126
CC-49	760	1400	2 min - T, C dwell	±0.00350	400	2,088
CC-50	760	1400	5 min - T, C dwell	±0.00300	250	2,503
CC-51	760	1400	5 min - T, C dwell	±0.00450	675	312
CC-52	760	1400	5 min - T, C dwell	±0.00625	1250	41
CC-53	927	1700	2 min - T, C dwell	±0.00300	1500	479
CC-54	927	1700	5 min - T, C dwell	±0.00356	2600	238
CC-55	927	1700	2 min - T, C dwell	±0.00200	550	727
CC-56	927	1700	2 min - T, C dwell	±0.00400	2300	94

Strainrange Partitioning concerns itself with inelastic material behavior, and for that reason the relationships of either total strain or elastic strain vs N_f are not scrutinized to the extent afforded the inelastic results (Section IV.D.3). Nonetheless, all engineering information which may facilitate the analysis of material response to complex thermal-mechanical cycling, must be considered.

1. Total Strain vs Life Relationships

Total strainrange, $\Delta\epsilon_t$ vs cyclic life, N_f plots are presented in figures 9 through 12. In general, increases in temperature result in decreases in life, at the same total strain. Exceptions to this are evident in the CP-type tests where the intermediate temperature 760°C (1400°F) lives exceed those of both the higher 927°C (1700°F) and lower 538°C (1000°F) temperatures, at equivalent total strains.

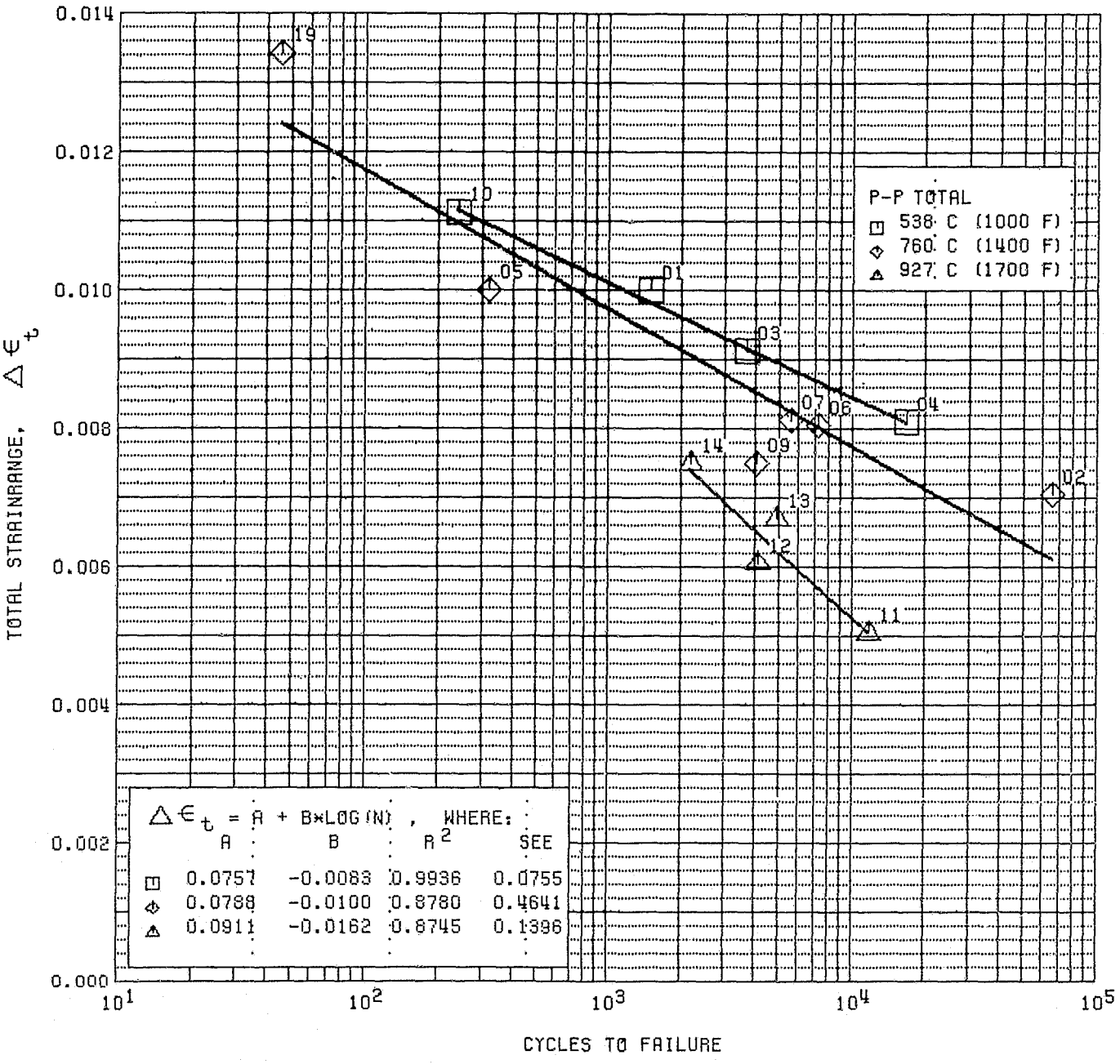

Figure 9. Total Strainrange vs Cycles to Failure, for PP-Type Tests on CA-101

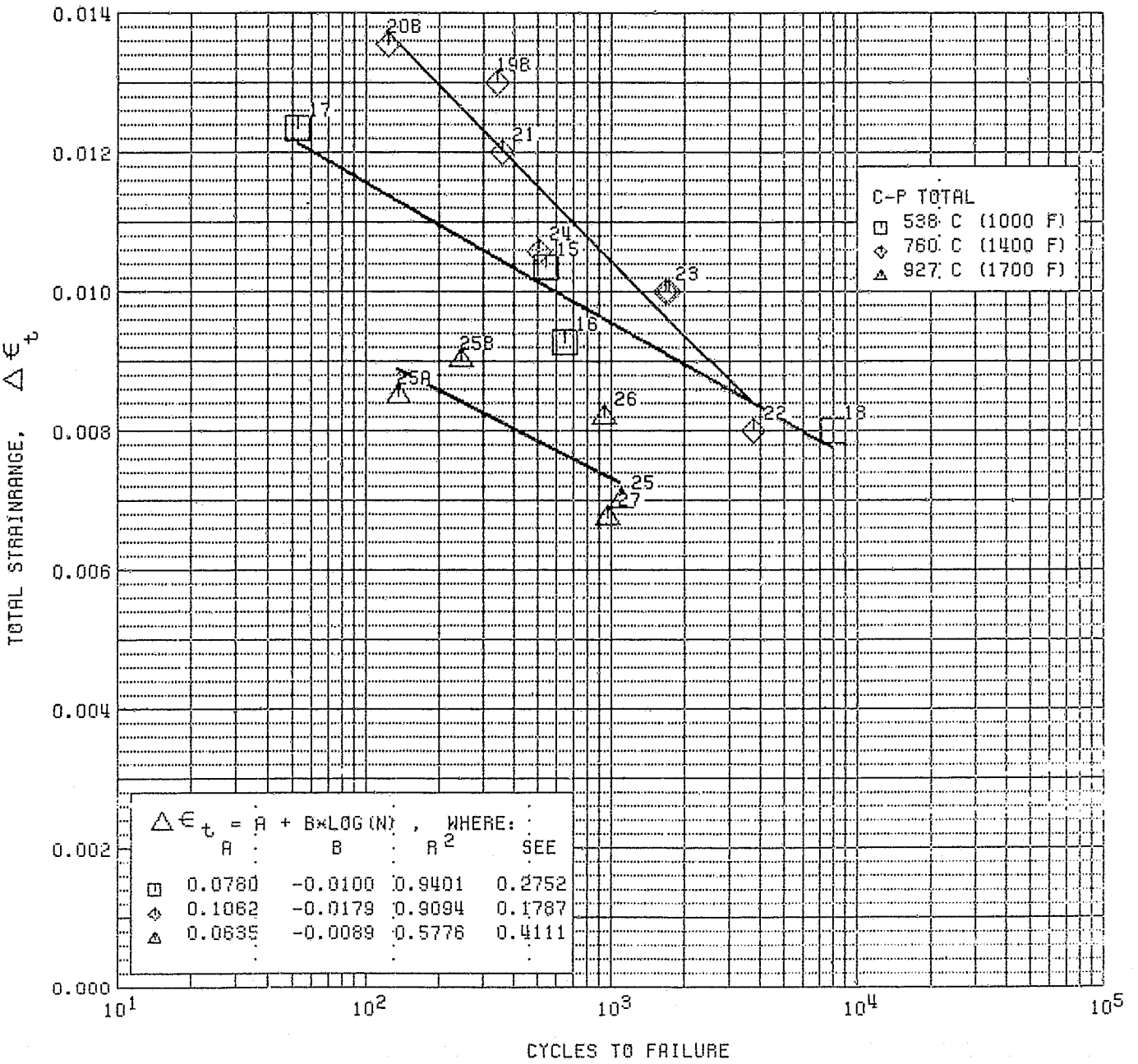

Figure 10. Total Strainrange vs Cycles to Failure, for CP-Type Tests on CA-101

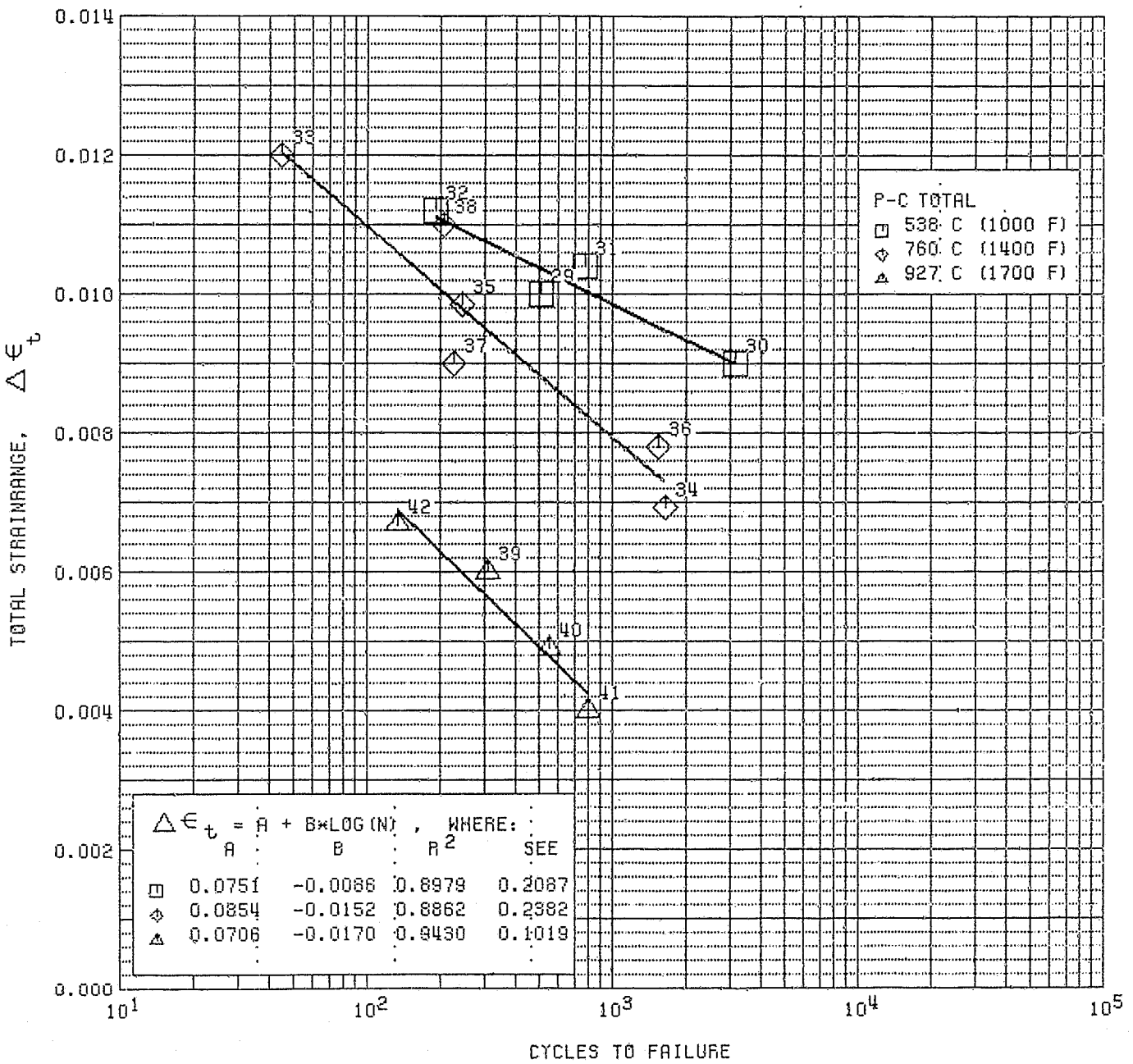

Figure 11. Total Strainrange vs Cycles to Failure, for PC-Type Tests on CA-101

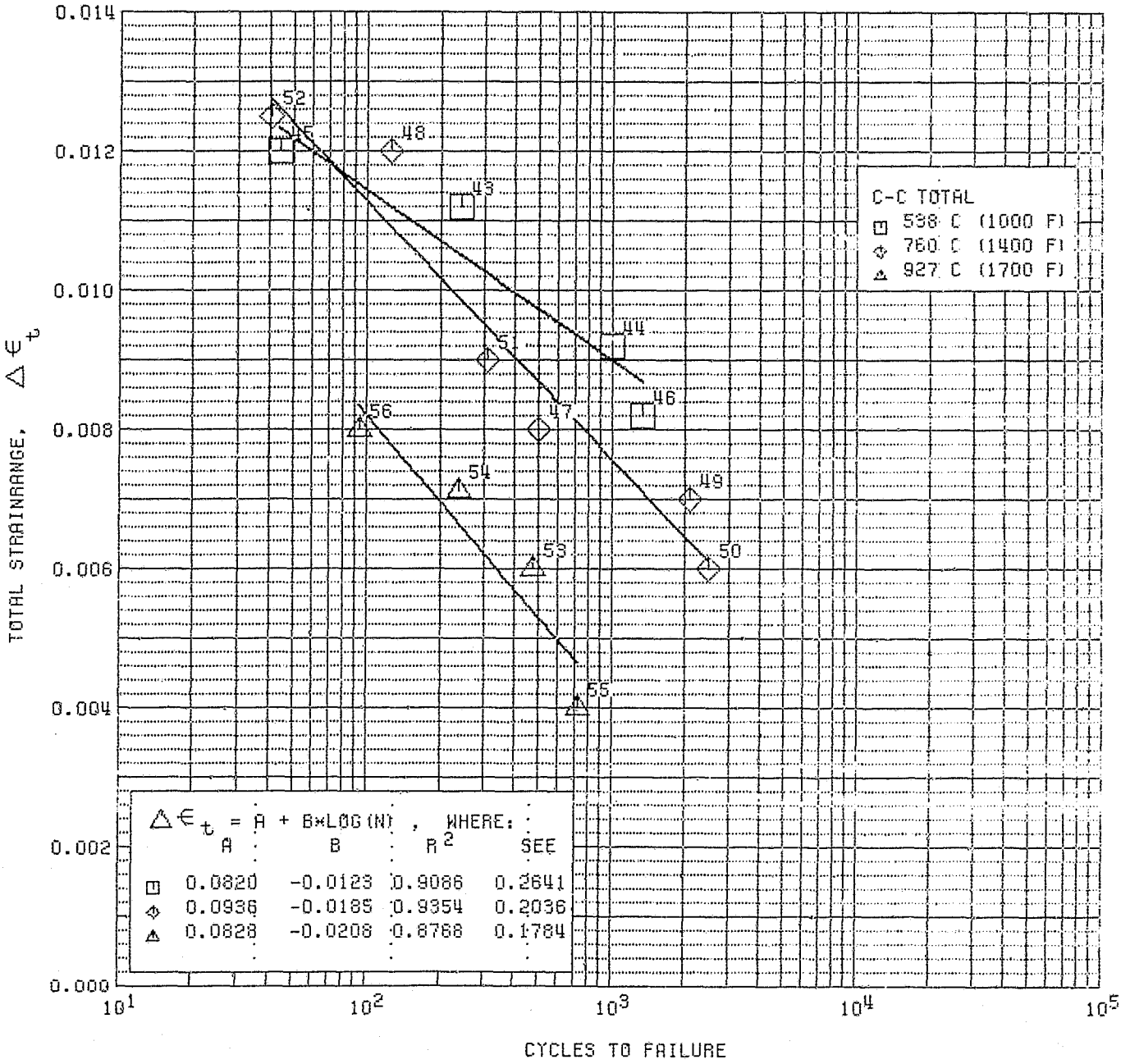

Figure 12. Total Strainrange vs Cycles to Failure, for CC-Type Tests on CA-101

There are other exceptions to the observation that life is inversely proportional to temperature: the intermediate and low temperature lines intersect at high total strains for CC-type tests, and approach intersection in PC-type tests. With all four cycle definitions, the high temperature, 927°C (1700°F), lives were shortest, at equivalent total strains, a direct consequence of the 40% decrease in yield strength between 760°C and 927°C (1400°F and 1700°F) as shown in table II.

2. Elastic Strain vs Life Relationships

Plots of elastic strainrange vs cyclic life (figures 13 through 16) are very similar to the previous plots of total strain (figures 9 through 12), because of the low ductility (small inelastic strains) of CA-101. Again the high temperature exhibited the lowest life at equivalent strains, and all observations concerning material response to total strain are valid for correlations with elastic strain.

3. Inelastic Strain vs Life Relationships

The cornerstones of Strainrange Partitioning are the thorough engineering, metallurgical, and statistical analyses of the material response to inelastic strains of the four generic types; PP, PC, CP, and CC. This Section, III.D.3, presents an integrated synopsis of these analyses.

Inelastic strainrange vs cycles to failure for each of the four basic cycle definitions are presented in figures 17 through 20. The equations describing each of these figures are least squares linear regressions, the statistics of which are included with each plot. An explanation of the statistical terminology is provided in Section V.A.1.

a. Metallurgical Analysis

Ideally, no cycle will yield lives greater than the PP-test. This is not the case for CA-101 as all basic types produce lives greater than the PP-type. Preliminary electron microscopy studies were performed to aid in the explanation of these results. Figure 21 presents thin-foil electron micrographs for specimens PP-5 (250 μin./in. 323 cycles), and CP-22 (350 μin./in., 3,783 cycles) both tested at 760°C (1400°F). Elementary dislocation networks are of approximately the same densities. However, CP-22 does reveal stacking faults that are associated with creep deformation. While this second active dislocation mechanism helps homogenize local deformation, it can also promote within-grain microfracture. Figure 22 shows scanning electron micrographs of the fracture surfaces of these same two specimens. This illustration shows that the fracture process for PP-5 is predominantly intergranular while that of CP-22 is mixed-mode. It is generally observed that cracks propagate slower in mixed modes than when propagation is primarily intergranular. Figure 23 presents results for PP-10 (325 μin./in., 240 cycles) and CP-18 (200 μin./in., 7,991 cycles) both tested at 538°C (1000°F). These scanning electron micrographs show that for specimen PP-10 the fracture surface is faceted indicating a brittle fracture. Specimen CP-18 indicates considerable flow on the fracture surface that could potentially retard crack growth.

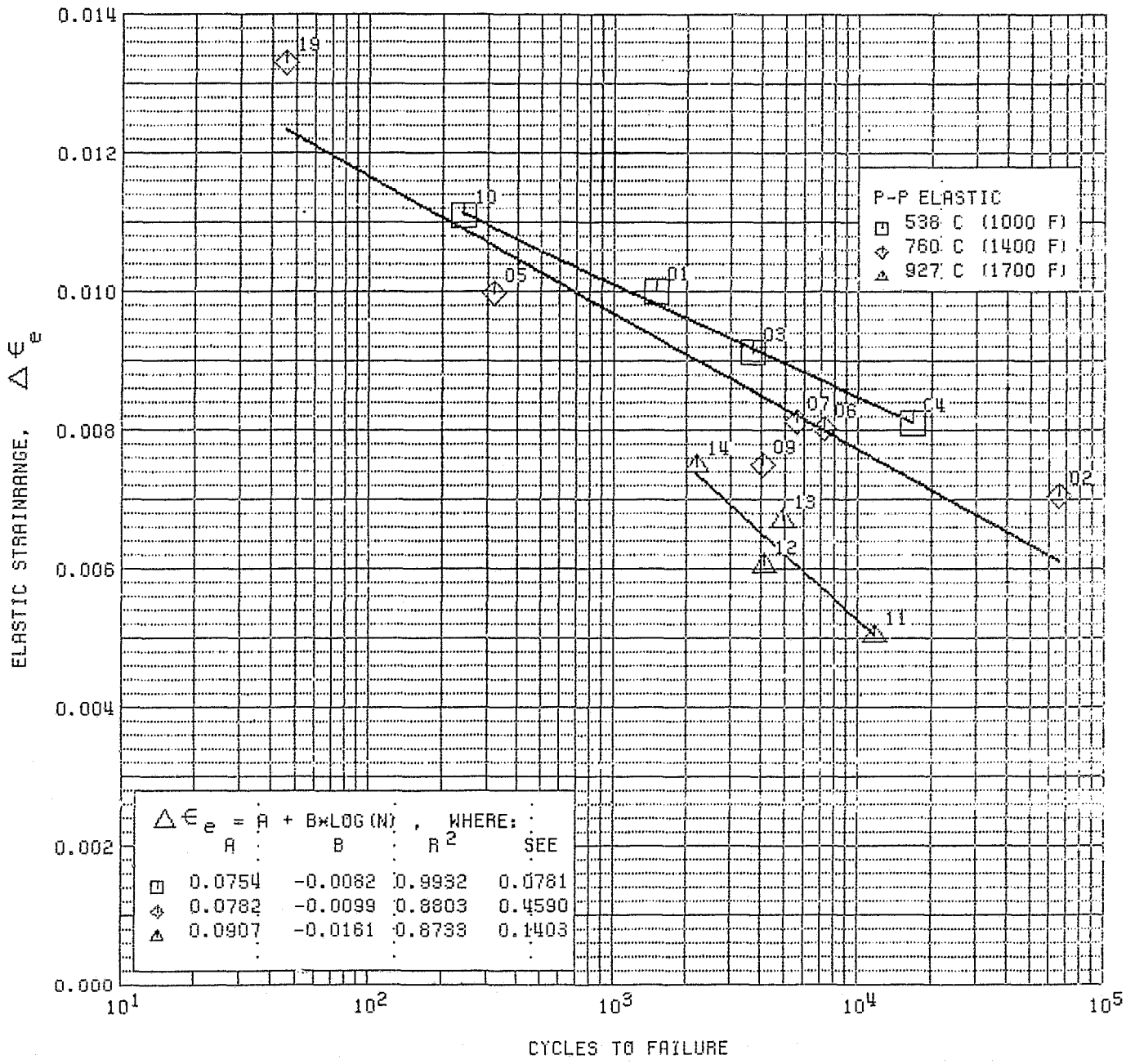

Figure 13. Elastic Strainrange vs Cycles to Failure, for PP-Type Tests on CA-101

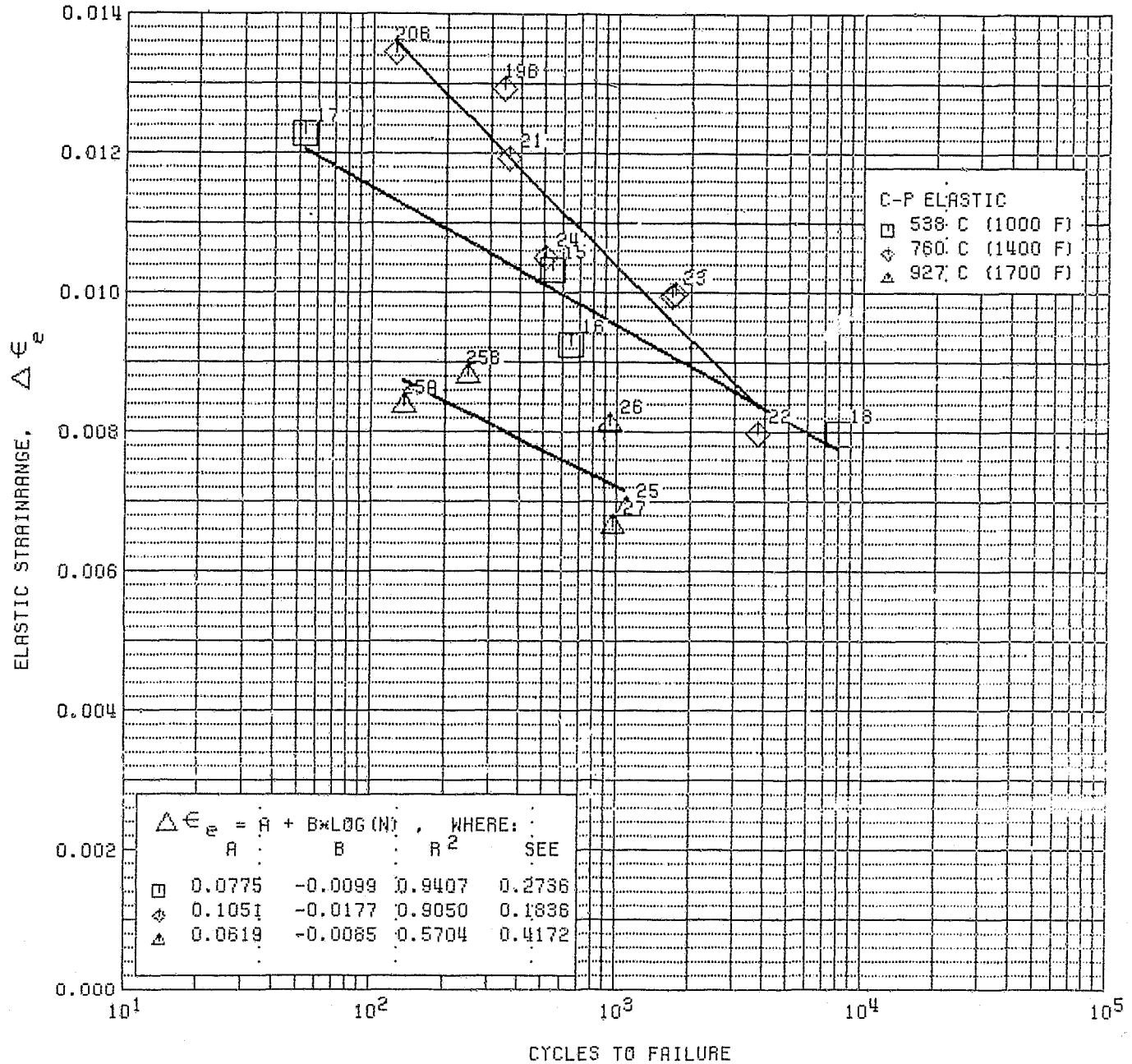

Figure 14. Elastic Strainrange vs Cycles to Failure, for CP-Type Tests on CA-101

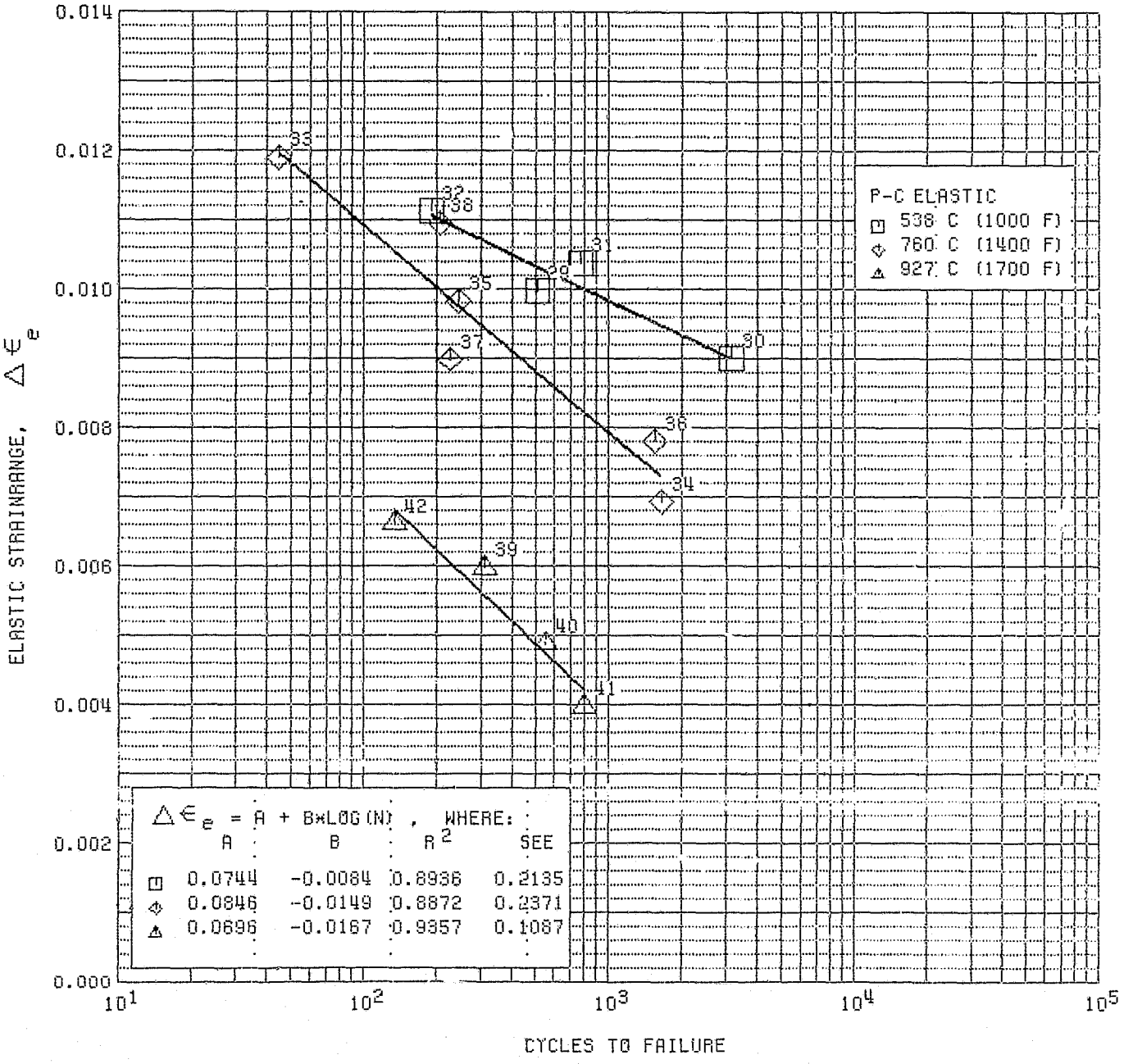

Figure 15. Elastic Strainrange vs Cycles to Failure, for PC-Type Tests on CA-101

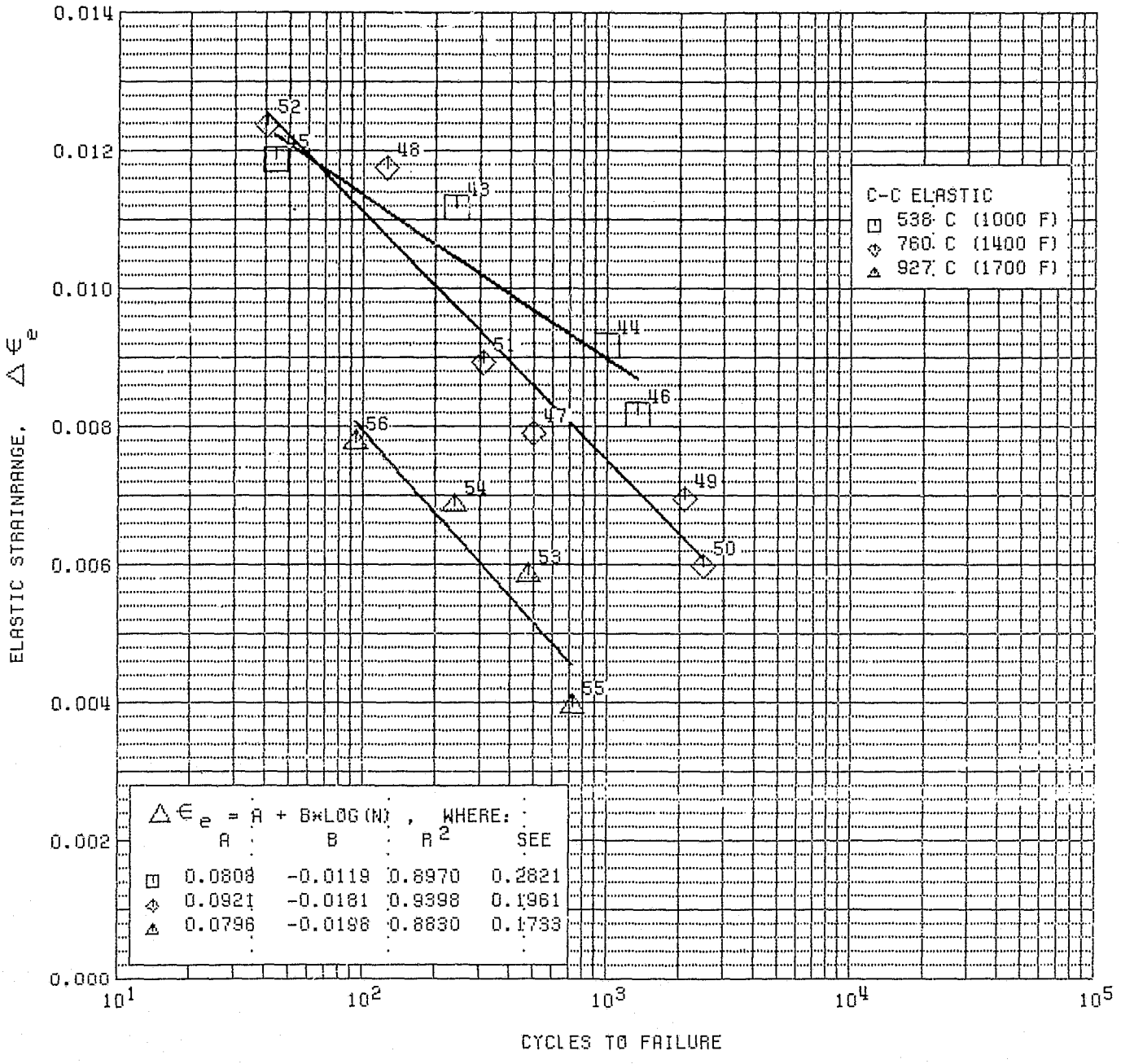

Figure 16. Elastic Strainrange vs Cycles to Failure, for CC-Type Tests on CA-101

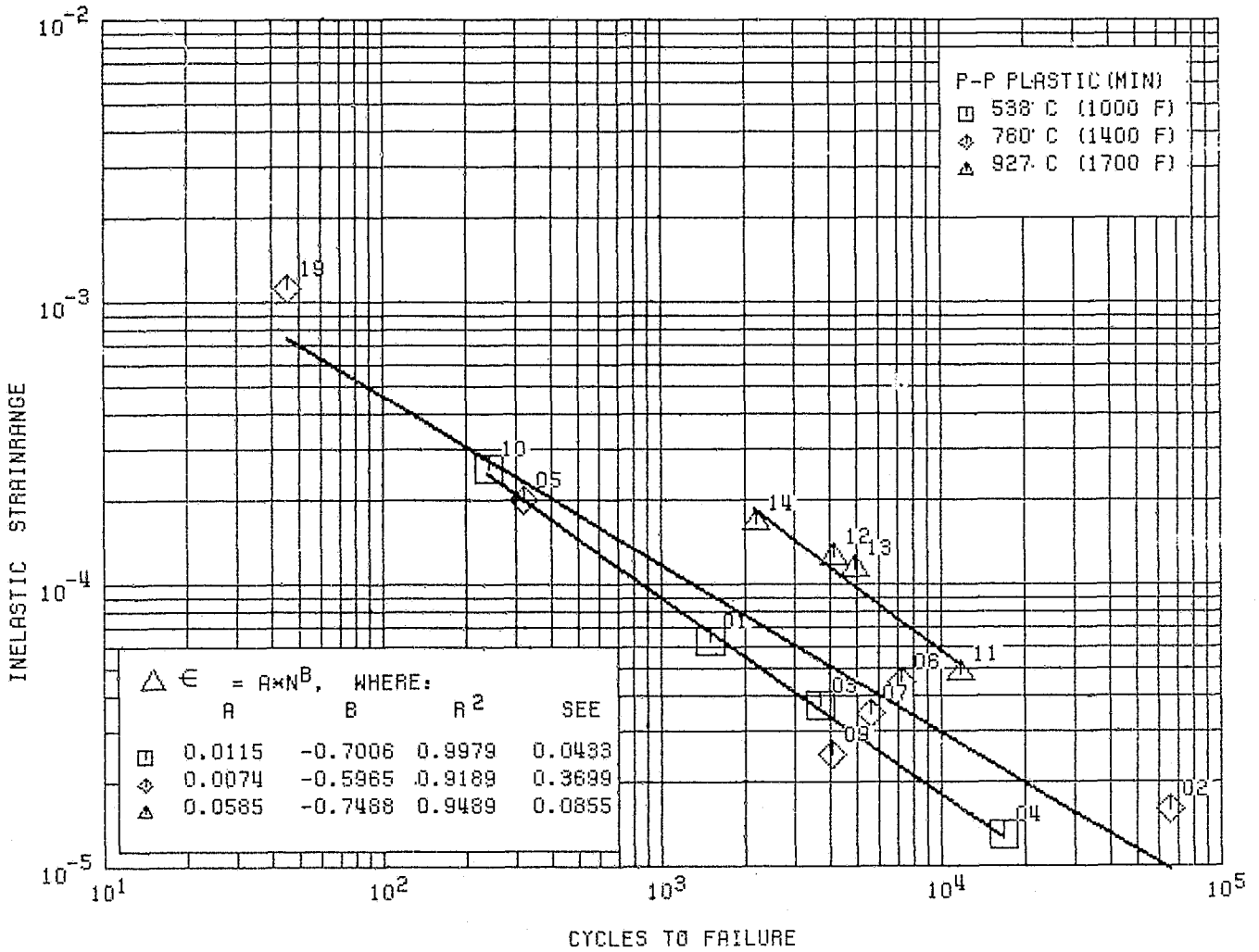

Figure 17. Inelastic Strainrange vs Cycles to Failure, for PP-Type Tests on CA-101

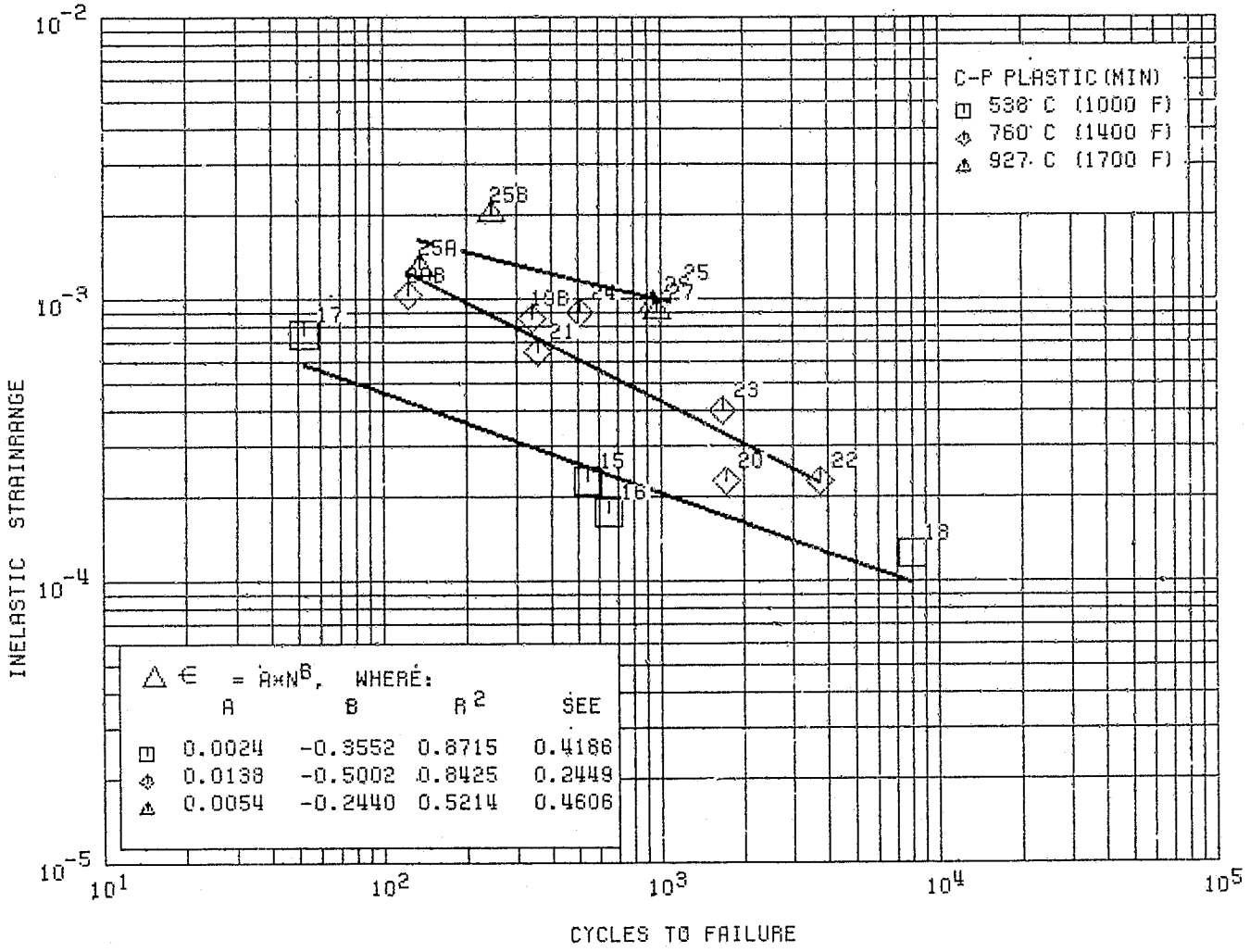

Figure 18. Inelastic Strainrange vs Cycles to Failure, for CP-Type Tests on CA-101

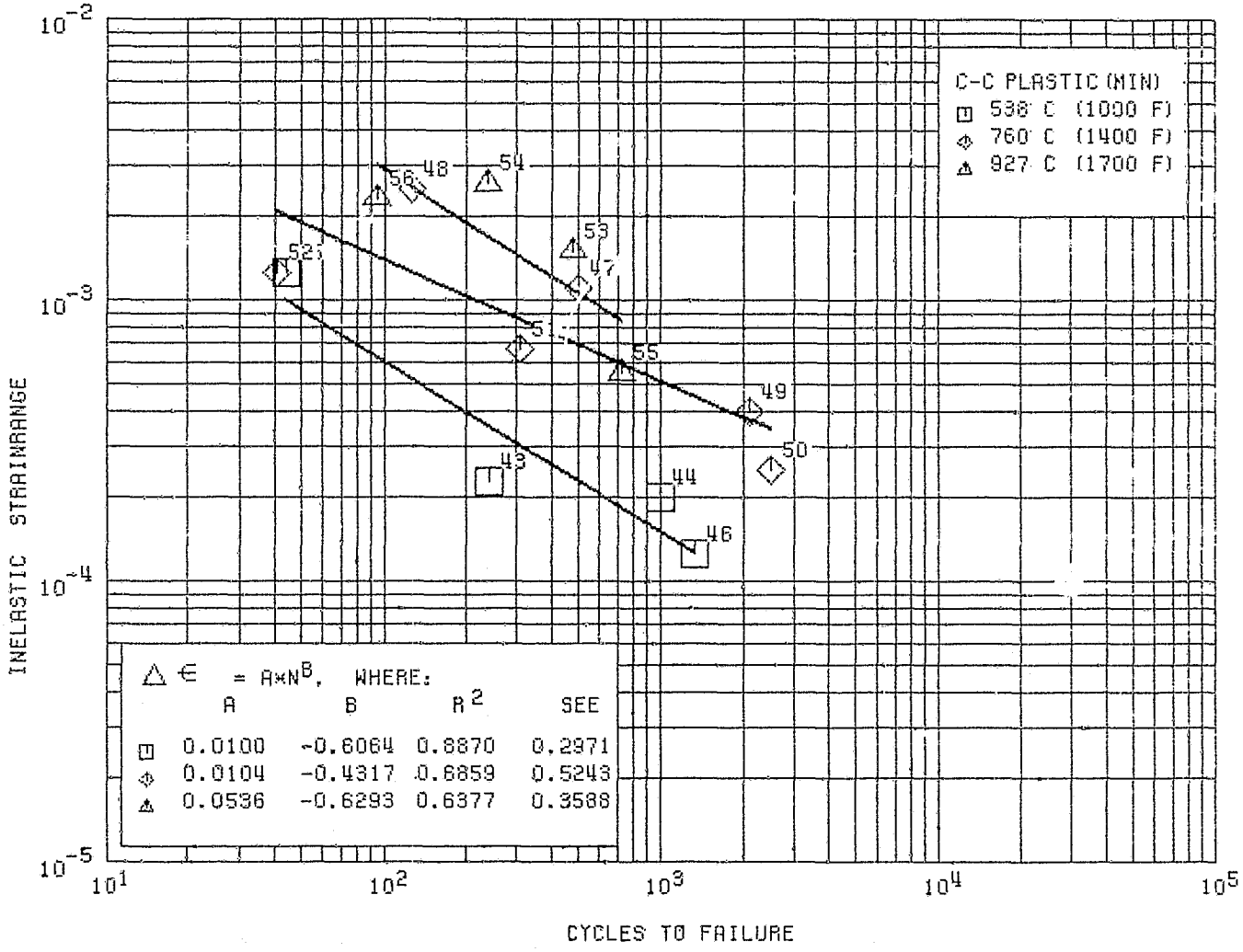

Figure 19. Inelastic Strainrange vs Cycles to Failure, for CC-Type Tests on CA-101

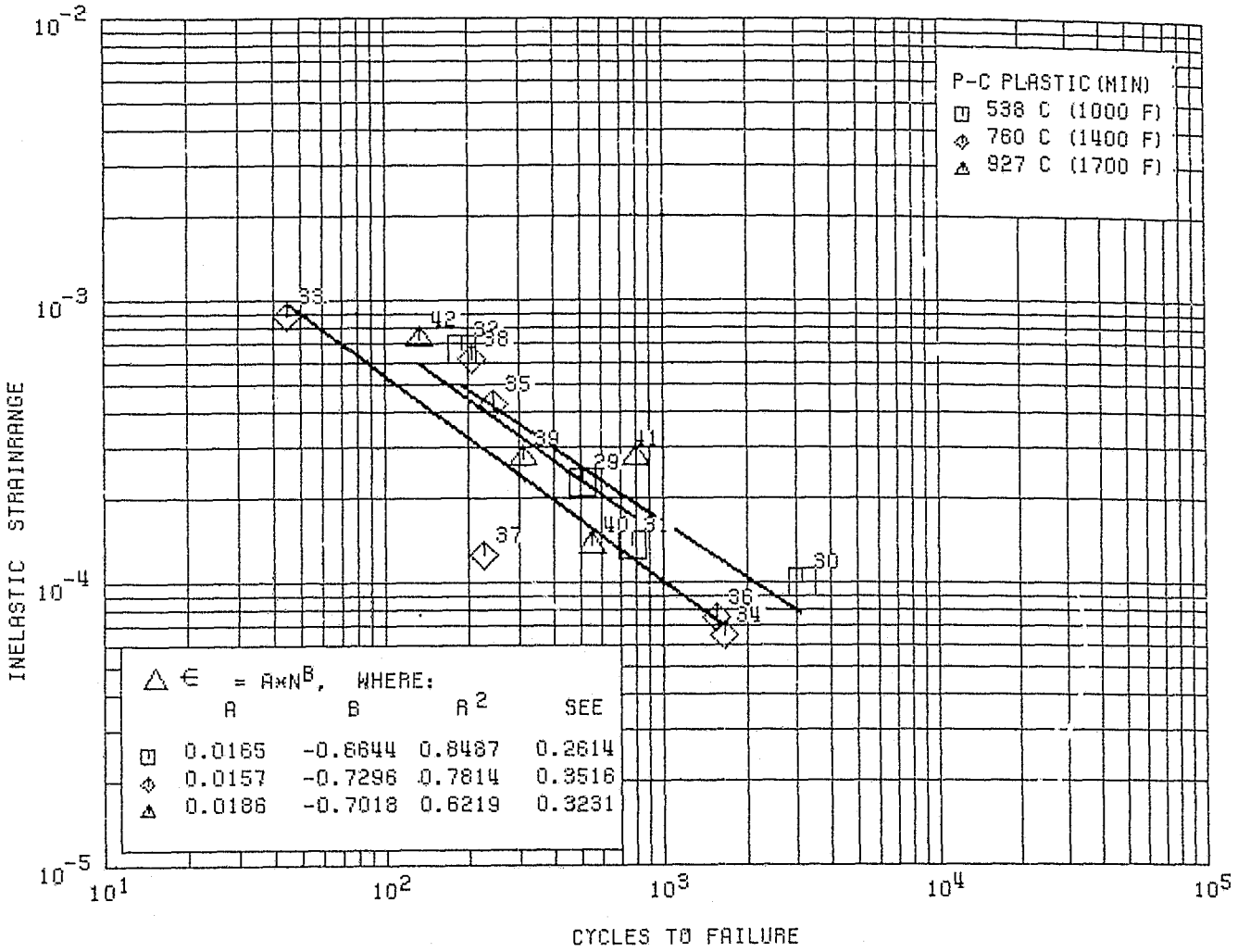

Figure 20. Inelastic Strainrange vs Cycles to Failure, for PC-Type Tests on CA-101

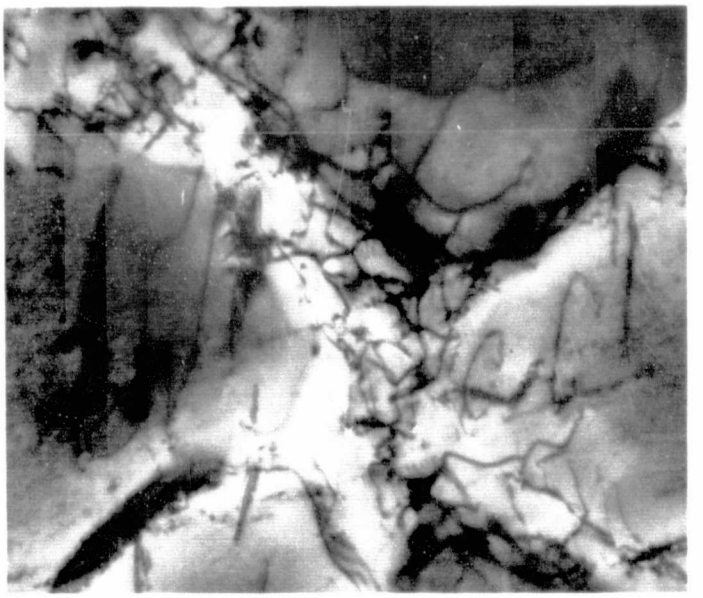

70,000X

PP-5

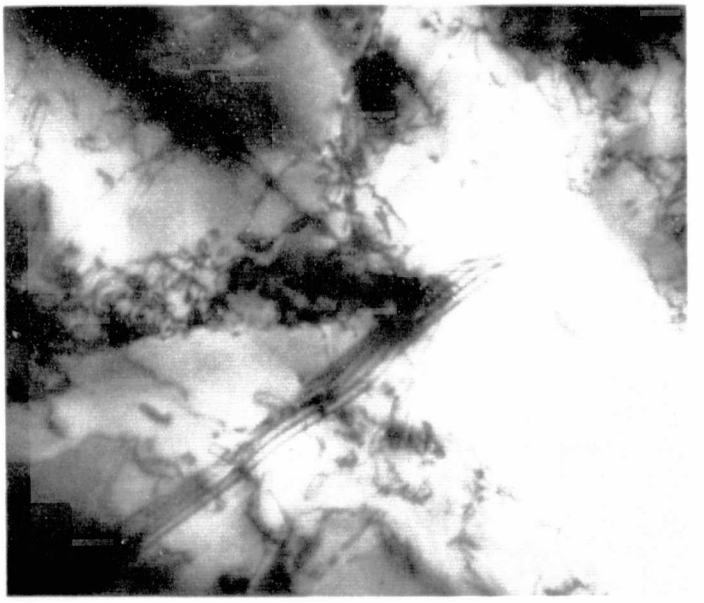

70,000X

CP-22

Figure 21. Thin-Foil Electron Micrographs for Specimens PP-5 and CP-22 FD 93338

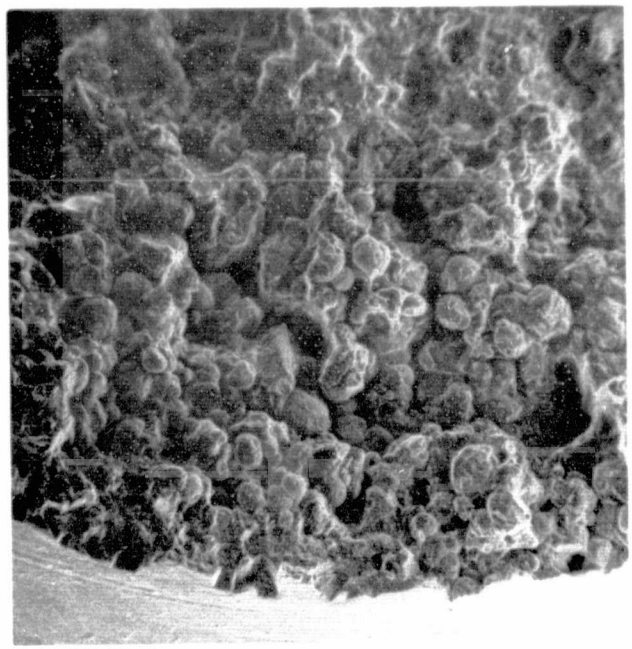

Mag: 40X PP-5

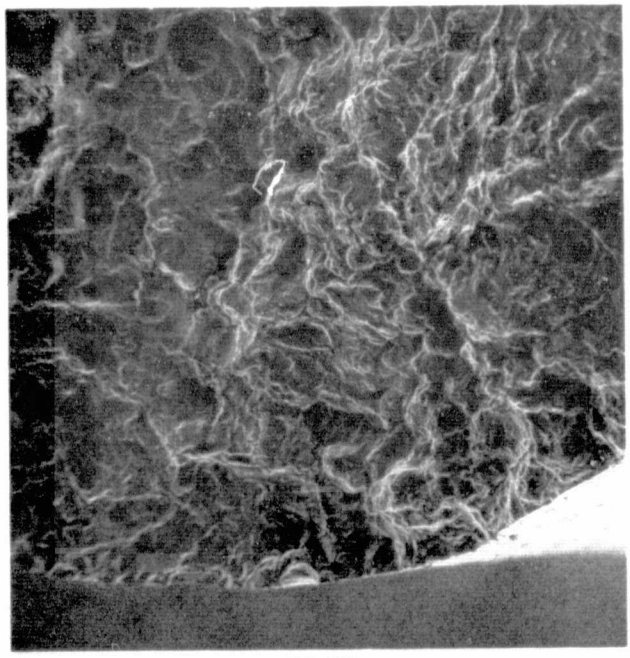

Mag: 40X CP-22

Figure 22. Scanning Electron Micrographs for Specimens PP-5 and CP-22 FD 93357

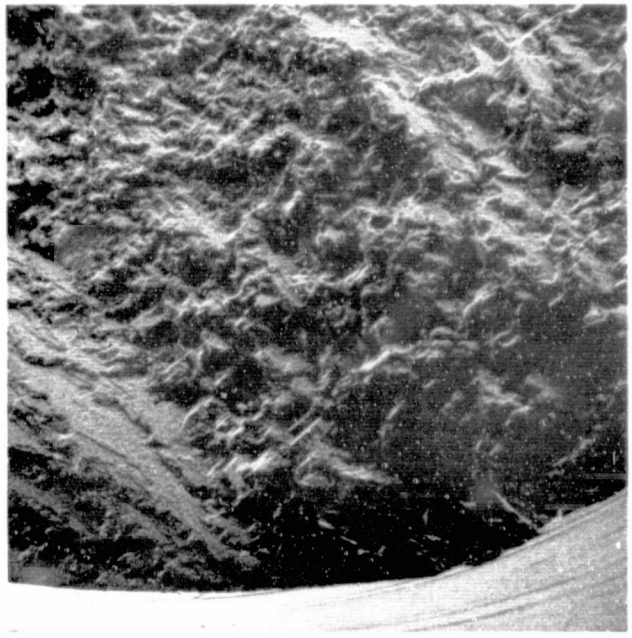

40X

PP-10

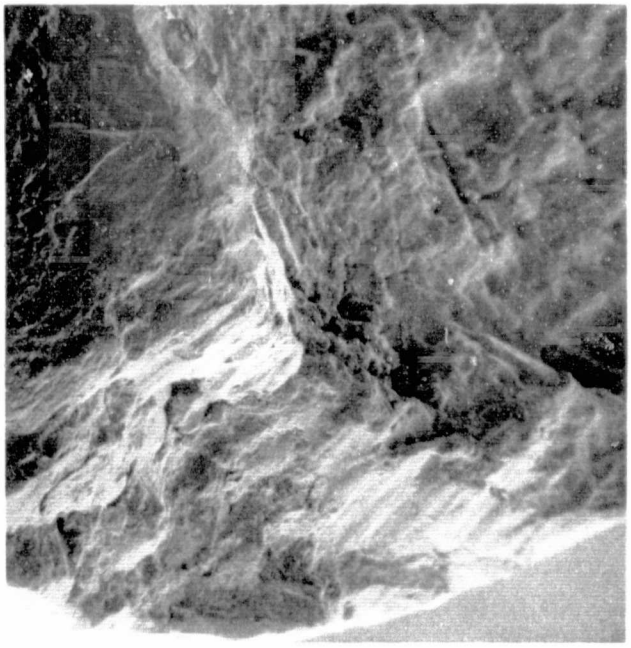

40X

CP-18

Figure 23. Scanning Electron Micrographs for Specimens PP-10 and CP-18 FD 93358

It is proposed, therefore, that the superposition of strain dwells in CA-101 alters both the initiation and propagation processes. Dwells can potentially retard the initiation process because of enhanced dispersion of localized deformation due to activation of secondary dislocation mechanisms, e.g., stacking faults. Dwells can potentially retard crack growth because of crack tip stress relaxation due to local creep deformation. Either one or both of these occurrences can lead to longer cyclic lives because of the presence of a dwell.

For this reason, in the presentation of PC, CP, and CC test results, cycles to failure are as measured with no allowance made for any P-P component. In addition to the metallurgical rationale just presented, there are two other, independent, reasons for assuming a negligible PP component in these tests: (1) The Interaction Damage Rule produces negative lives when used in subtracting any sizable PP component. This unexpected result is discussed in detail in Section V.C, and (2) measured fractions of PP-type inelastic strain, determined during the incremental partitioning (IP) test phase, were small even for saw-tooth waveforms. Section V.B discusses IP results.

b. Analysis of the Four Generic Test Types

Results of each of the four generic test types are presented as $\Delta\epsilon_i$ vs N_f as follows:

1. Figure 17 presents the linear regressions describing $\Delta\epsilon_{pp}$ vs N_f. Increasing temperature is seen to increase the amount of tolerable PP-type strain, $\Delta\epsilon_{pp}$, at any given cyclic life, N_f. Viewed differently, at any given $\Delta\epsilon_{pp}$, increasing temperature increases N_f. The slopes of each line (numerical values are included with each plot) are not equal, however, and extrapolations to $N_f = 1$ cycle show the intermediate temperature of 760°C (1400°F) line intersecting at the lowest $\Delta\epsilon_{pp}$, and the relative position of the temperatures to be the same as observed for tensile ductility (Section III.B and C). The implications of this inelastic strainrange positioning with respect to temperature will be discussed in Section V.A.1. The reader is to be cautioned that these slopes are based on relatively sparse data and extrapolations beyond the range of data are dangerous. The extrapolation discussed is for qualitative comparisons only.

2. Figure 18 graphically depicts CP-type test results, $\Delta\epsilon_{cp}$ vs N_f. The effect of increasing temperature is similar to that observed with PP and CC tests: increasing temperature increases N_f at equivalent values of $\Delta\epsilon_{cp}$ within the range of data. This trend would not hold outside the data range because the slopes of the respective linear representations are unequal and extrapolations would result in intersection lines. The decidedly shallower slope exhibited at 927°C (1700°F), as a result of the behavior of specimens 25A and 25B, is discouraging. No apparent anomalies exist in these two tests, so the computed slope must be excepted, although its shallowness is a result of data scatter rather than any real physical phenomenon.

Because the PC tests exhibited behavior unlike that of the other three generic test types, these tests will be discussed last.

3. The results of CC-type tests are presented in figure 19. As with PP and CP tests; increasing temperature allowed greater cyclic life at any given strainrange. The slopes at the high and low temperatures, 927°C and 538°C (1700°F and 1000°F) are nearly equal and are steeper than that observed at the intermediate temperature, 760°C (1400°F). The difference is attributed to data scatter.

4. The behavior of the PC tests, as a group, is decidedly unlike that of the other three test definitions (figure 20). Most notable unlike that of the other three test definitions. Most notable is the effect of temperature. There is only about a factor of two difference in cyclic life attributable to temperature throughout the entire range of data. By comparison the other test definitions display an order of magnitude difference in cyclic life between high and low temperatures. The position of the temperature lines is unusual, with cyclic life increasing as temperature changed from intermediate 760°C (1400°F) to high 927°C (1700°F) to low 538°C (1000°F). Recall that the usual order, was high to low: when temperature increases, cyclic life increased, $\Delta\epsilon_i$ being constant. On the other hand, data scatter for PC-type tests is comparatively small, and all three temperature lines exhibit nearly equal slopes.

Figures 17 through 20 presented inelastic strainrange data grouped according to test cycle definition. Figures 24 through 26 present this same data grouped isothermally; some interesting results appear.

5. Figure 24, presents inelastic strainrange vs cycles to failure for all four cycle definitions at low temperature 538°C (1000°F). The most salient feature of this plot is the position of the PC line, far to the right (greater life) of the others. This is a direct consequence of the compressive mean stress resulting from the dwell in compression. Because PC specimens operated at a lower mean stress than the other three tests, they survived longer at this low temperature where no appreciable relaxation in compression could occur.

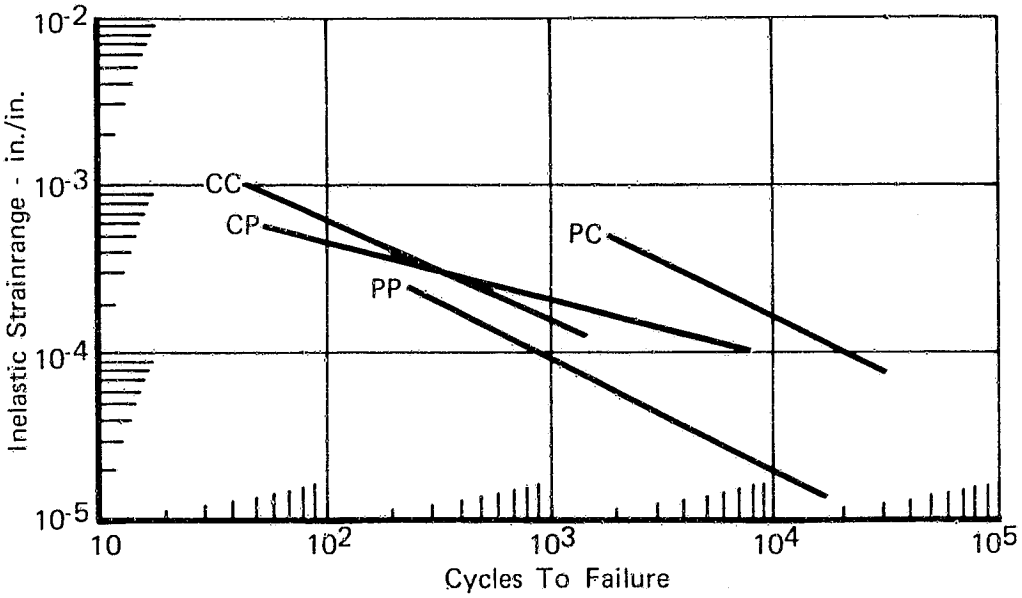

Figure 24. Comparison of $\Delta\epsilon_i$ vs N_f for Each of the Generic Test Types at 538°C (1000°F) FD 95915

It is interesting to note that PP, CC, and PC tests exhibit similar slopes even though there is a sizable (factor of 20) difference in cyclic life, at constant $\Delta\epsilon_i$. The shallower slope observed in CP data maybe explained as follows: during CP loading, at 538°C (1000°F), tensile stress is allowed to relax somewhat thereby permitting some homogenization of the localized deformation produced by the imposition of the tensile load. However, when the total strain is relatively high (0.9% to 1.2%) the deleterious effect of the initial high tensile load outweighs the potentially beneficial effects of load (stress) relaxation. Therefore, at high inelastic strains, corresponding to high tensile loads, the cyclic lives are short, approaching PP lines, and at low inelastic strains, CP lives increase, exceeding those of PP and CC, and approaching PC.

6. Figure 25 presents inelastic strainrange vs cyclic life for all four test definitions at high temperature, 927°C (1700°F). Here, the PC tests are seen to fail before any others at a given inelastic strainrange. The increased material ductility at this temperature permits considerable compressive stress relaxation during dwell, (compared to that observed at low temperature 583°C (1000°F)) resulting in an ever increasing mean stress, and early failure.

   Again, PP, PC, and CC tests displayed similar slopes with CP tests exhibiting a shallow slope for reasons previously discussed.

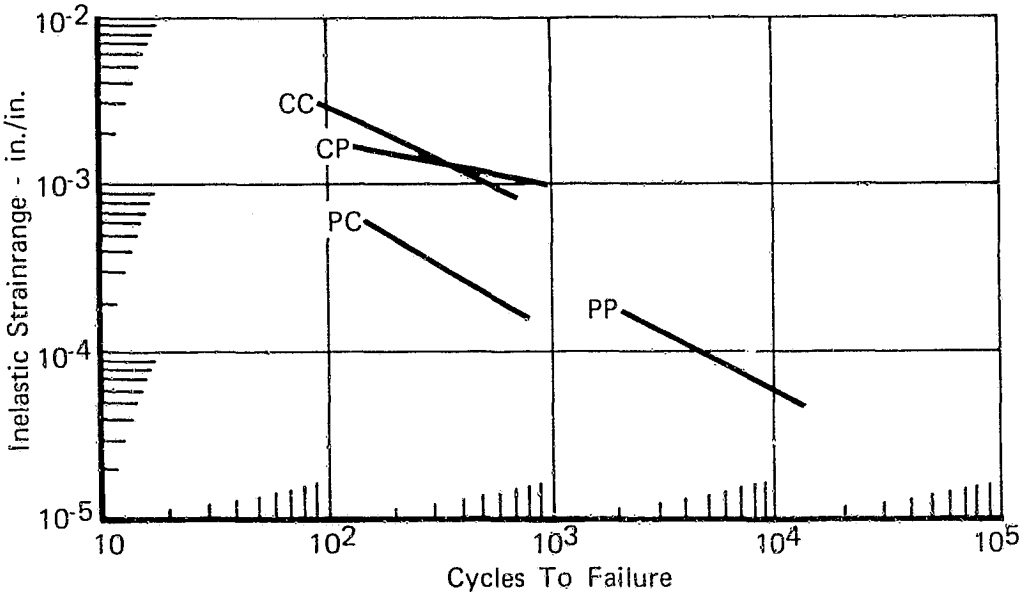

Figure 25. Comparison of $\Delta\epsilon_i$ vs N_f for Each of the Generic Test Types at 927°C (1700°F) FD 95916

7. The intermediate temperature, 760°C (1400°F), test results $\Delta\epsilon_i$ vs N_f are presented in figure 26.

   At this temperature the PP and PC tests behave similarily, having nearly coincident lines. In a similar manner the two tests which experienced tensile stress relaxation, CP and CC, also displayed behavior similar to one another. The immediate conclusion is that at 760°C (1400°F) any effect of the compressive dwell is almost indiscernable; tests reversed with a dwell in compression show little difference from those reversed with the 1 Hz saw-tooth only.

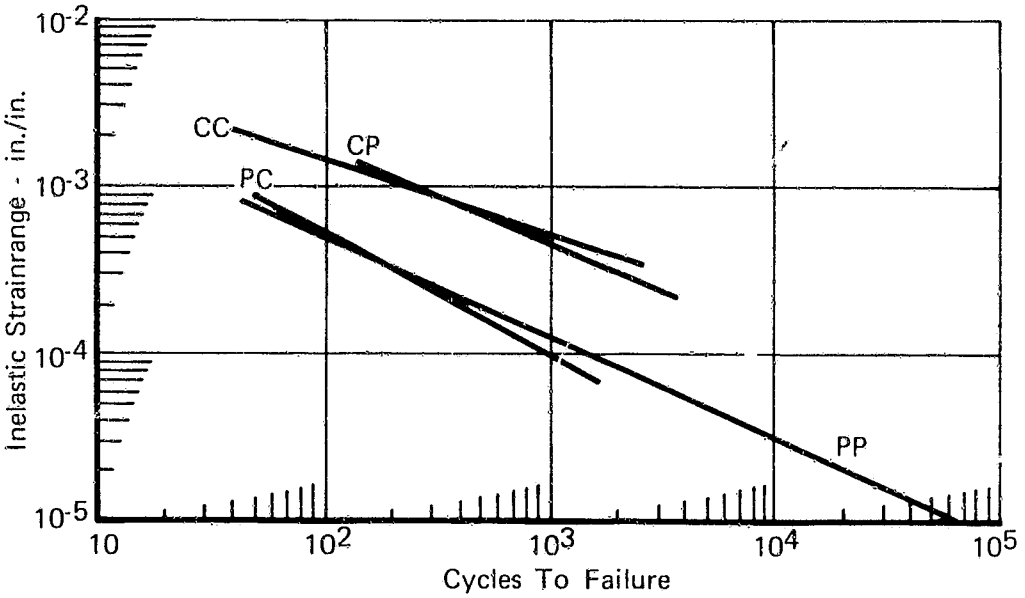

Figure 26. Comparison of $\Delta\epsilon_i$ vs N_f for Each of the Generic Test Types at 760°C (1400°F) FD 95917

SECTION V
TASK II - INTERPRETATION, CHARACTERIZATION, AND LIFE PREDICTIONS

A. EXPLANATION AND JUSTIFICATION OF STATISTICAL NORMALIZATION

Inelastic strainrange vs cycles to failure for the four basic tests are shown in figures 17 through 20. The PP results are shown in figure 17. It is immediately noticeable that the three lines representing 538°C, 760°C, and 927°C (1000°F, 1400°F, and 1700°F) have decidedly unequal slopes. This means that dividing $\Delta\epsilon_i$ by tensile ductilities would produce data which may be regressed as a single family, but would ignore any real differences in material behavior at differing temperatures.

In addition, the relative position ($\Delta\epsilon_i$ at N_f = constant) of these temperatures is 927°C, 760°C, and 538°C (1700°F, 1400°F, and 1000°F) in the range of observed data. However, extrapolations of these individual lines to N_f = 1 cycle, show a relative repositioning of temperatures. The extrapolated "ductilities" at one cycle are in decreasing order 0.0585, 0.0115, and 0.0074 at 927°C, 538°C, and 760°C (1700°F, 1000°F, and 1400°F). The tensile ductilities presented previously (Section III B and C) also show this trend: ductility (2%) at 760°C (1400°F) is less than the ductility at either the higher (7%) or the lower (3%) temperature with the highest ductility (7%) occurring at the highest temperature 937°C (1700°F). One must conclude that the observed differences in slope are real, and are not artifacts of the data scatter.

1. Mathematical Explanation of Statistical Normalization

The foregoing discussion illustrates the difficulties in ductility normalization of three temperatures into one linear representation of material behavior. Consider the meaning of the parameter, $\Delta\epsilon_i/D$. This may be interpreted as the ratio of observed inelastic strainrange to that strainrange which results in failure at one cycle. At one cycle, D could be considered as the material cyclic ductility. Using the concept of D as the maximum amount of tolerable deformation during cyclic straining, the relative values of D at different temperatures can be inferred from the relative position of the temperature lines on the $\Delta\epsilon_i$ vs N_f plots for each of the four basic LCF cycle definitions.

An algorithm was developed which permits simultaneous computation of the "ductilities" and the linear regression coefficients. Values for D were selected such that the summed squared error[1] between $\Delta\epsilon_i/D_{observed}$[2] and $\Delta\epsilon_i/D_{calculated}$[3] is a minimum. The values of the linear regression coefficients, A and B, were similarly computed as those values which minimized the summed squared error between $N_{f\,observed}$ and $N_{f\,calculated}$[4] Notice that strain

---

[1] When $y_{j,\,calculated} = f(x_j)$, the "summed squared error" is defined as $\sum_{j=1}^{n} (y_{j,\,calculated} - y_{j,\,observed})^2$, where n is the number of data pairs.

[2] Value of "ductility" normalized strainrange observed to cause failure at N_f cycles.

[3] Value calculated from the linear relationship, $\Delta\epsilon_i/D = A\,N_f^B$.

[4] $N_{f\,calculated}$ is computed by inverting the previous equation to give:

$$N_f = \left(\frac{\Delta\epsilon_i/D}{A}\right)^{1/B}$$

(Y) "errors" are calculated vertically, and life (X) "errors" horizontally, when referring to the standard X-Y representation of these parameters.

Values for D_{1700}, D_{1400}, A, and B were computed by simultaneous solution of the four equations which result from differentiating the squared error equations with respect to the appropriate variables, and equating these derivatives to zero. As previously mentioned, the relative position of the temperature lines permits computation of relative values of D. It is therefore necessary to fix one value in order to compute the others from their relative position. For this reason D_{1000} was defined as 0.02, a value approximately equal to the 538°C (1000°F) tensile ductility.

2. Presentation of Normalized Data

Figures 27, 29, 31, 33, and 35 present the "ductility" normalized relationships. Values for D and the regression coefficients A, and B are included on each computer plot, as well as the statistics of the fit; SEE is measured horizontally and has units of log cycles.

It must be remembered, that "ductility," D, has been included in these relationships, and must be considered when reading each curve. To determine the cyclic life expected under some known type of inelastic strainrange and temperature, the appropriate value of D must first be determined. Next, the "ductility" normalized inelastic strainrange parameter, $\Delta\epsilon_i/D$, is calculated. Entering the appropriate curve (PP, PC, CP, or CC), with this parameter, the expected cyclic life can be read directly.

Figures 28, 30, 32, and 34 provide a graphic comparison between observed cyclic life and that computed from the regressions discussed above. The overall statistics of the fit, calculated using all three temperatures are presented on these plots.

The behavior of each test was discussed in detail in Section IV. D. 3, and a synoptic presentation of that analysis is given graphically by figure 35, "ductility" normalized inelastic strainrange vs cyclic life, for all four generic cyclic definitions.

PP-type tests are the most severe; PP lives are shorter in every case than the other test definitions at equivalent normalized strainranges, $\Delta\epsilon_i/D$. Because values for D are functions of test definition in addition to test temperature, only general conclusions can be drawn. At high $\Delta\epsilon_i/D$, tests containing compressive dwells (PC, CC) have longer cyclic lives than tests with 1 Hz sawtooth in compression (PP, CP). This trend is reversed at lower values of $\Delta\epsilon_i/D$. The shallow slope of the CP line is again evident.

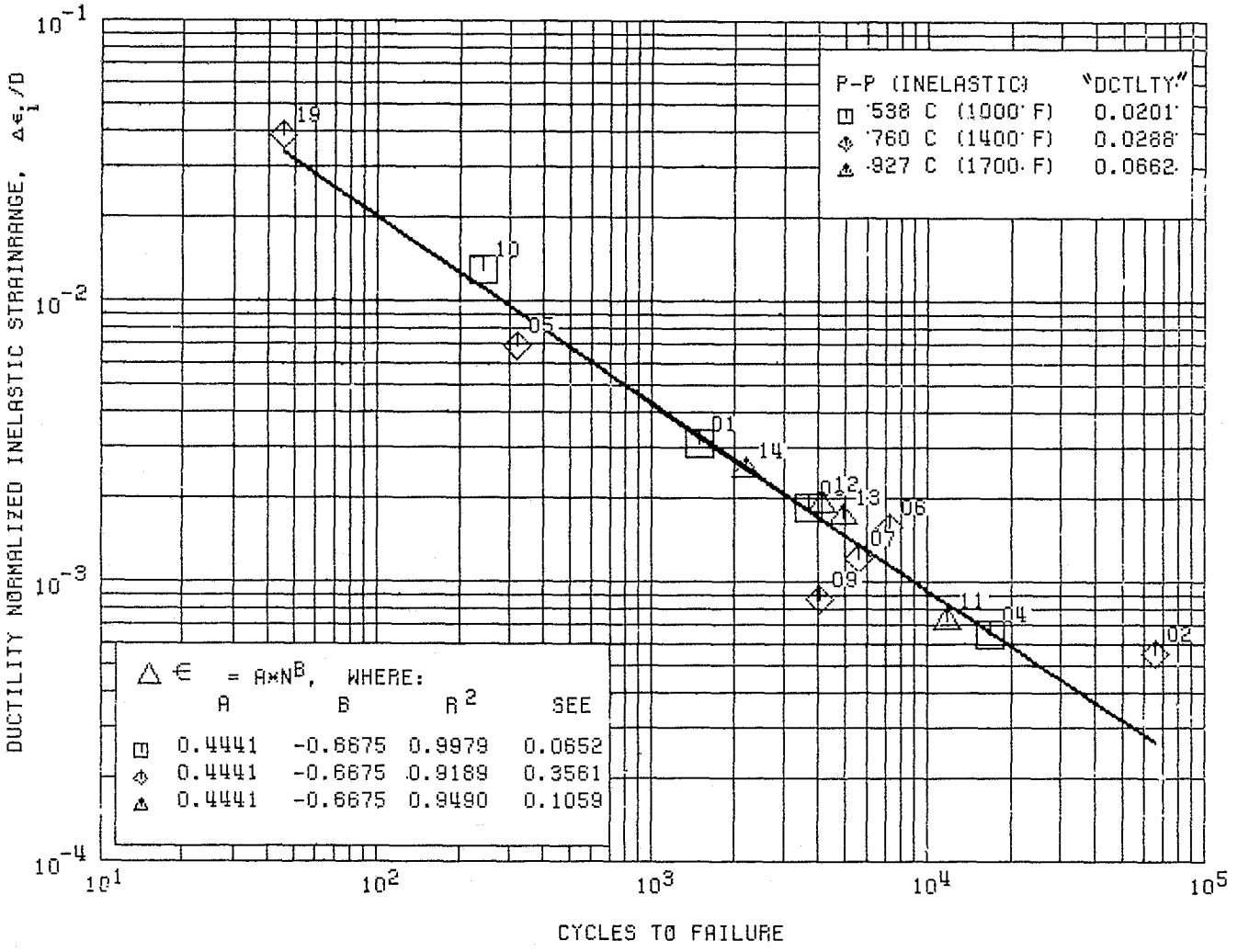

Figure 27. "Ductility" Normalized Inelastic Strainrange vs Cycles to Failure, for PP-Type Tests on CA-101

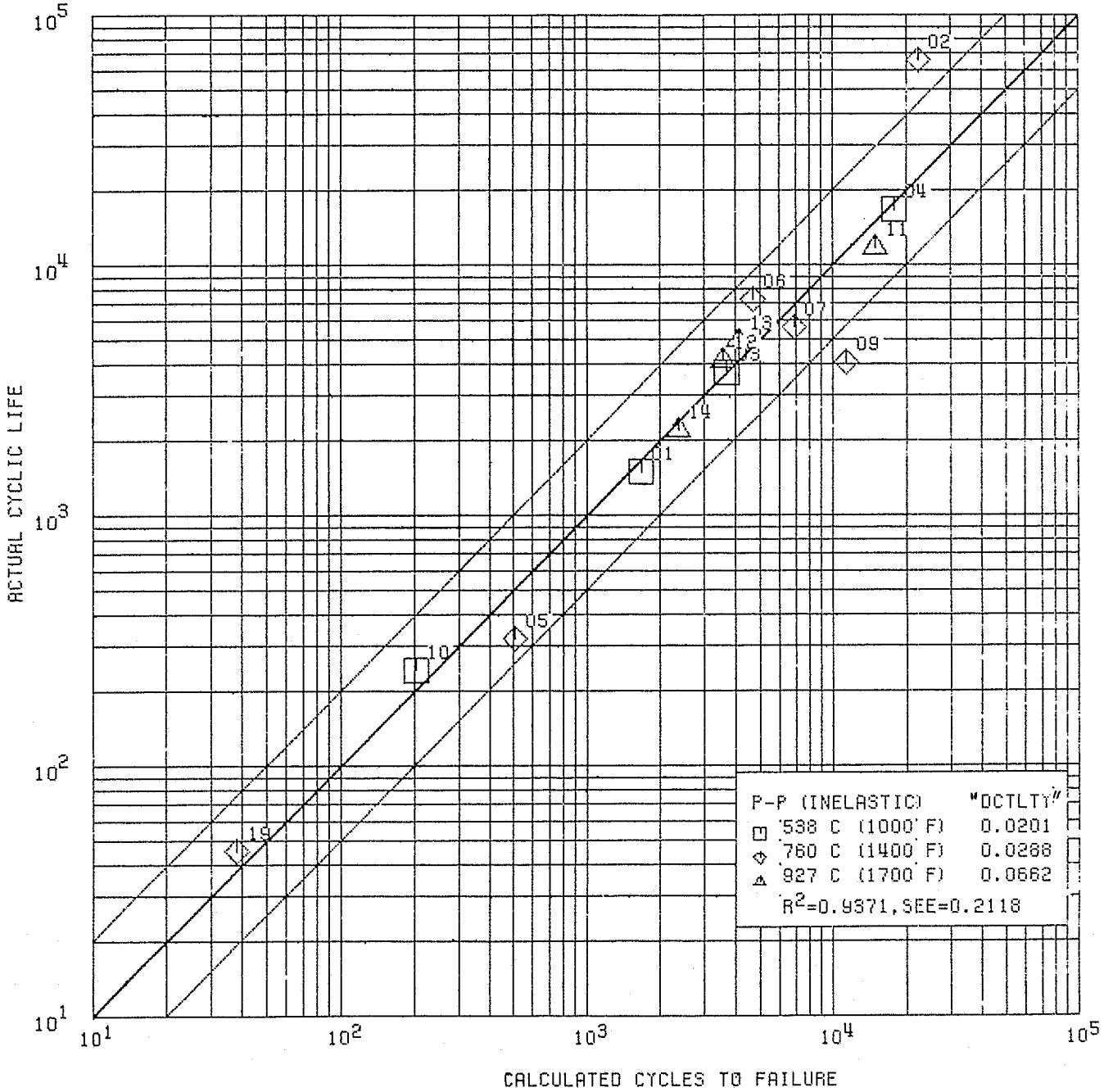

Figure 28. Actual vs Calculated Cyclic Life, for PP-Type Tests on CA-101

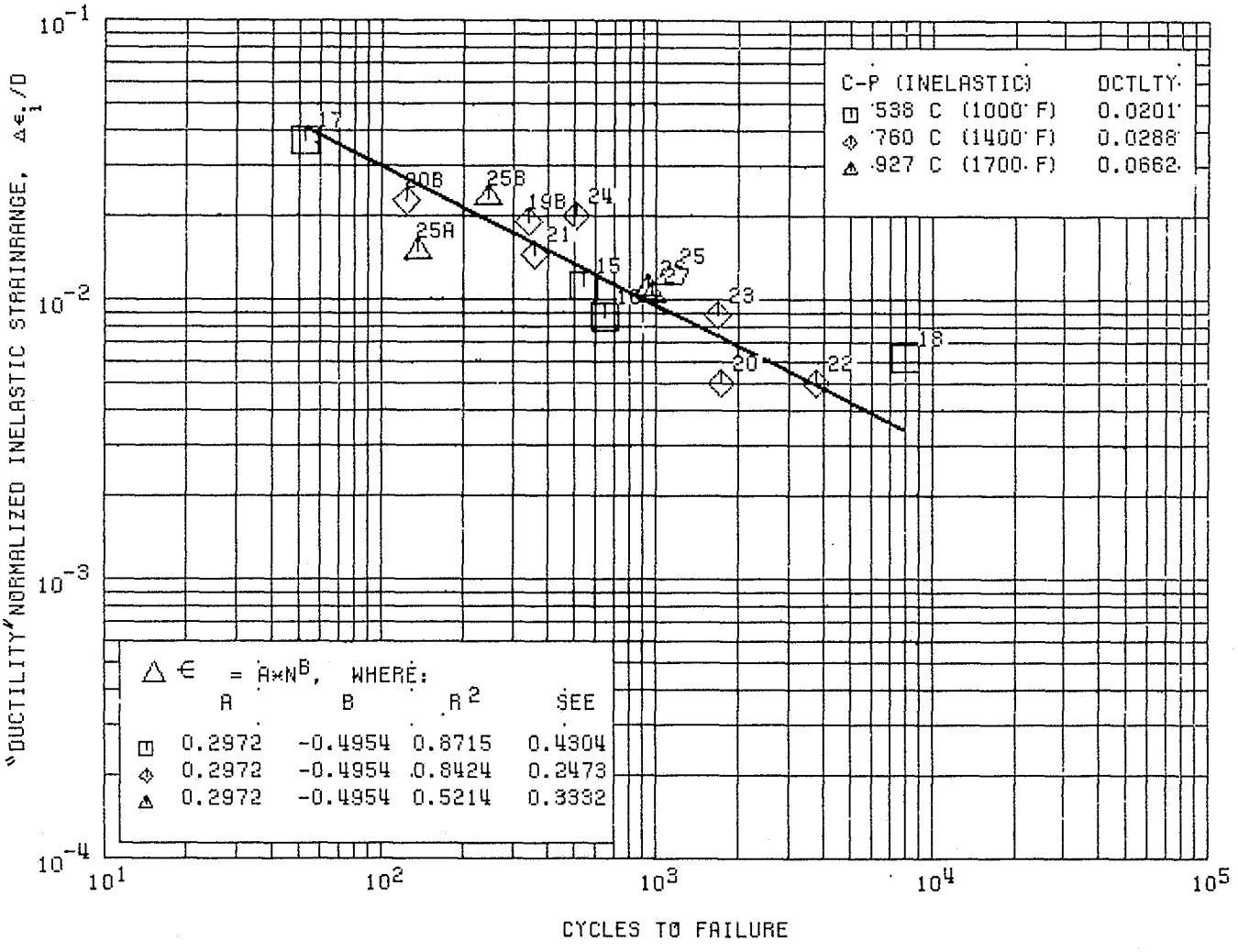

Figure 29. "Ductility" Normalized Inelastic Strainrange vs Cycles to Failure, for CP-Type Tests on CA-101

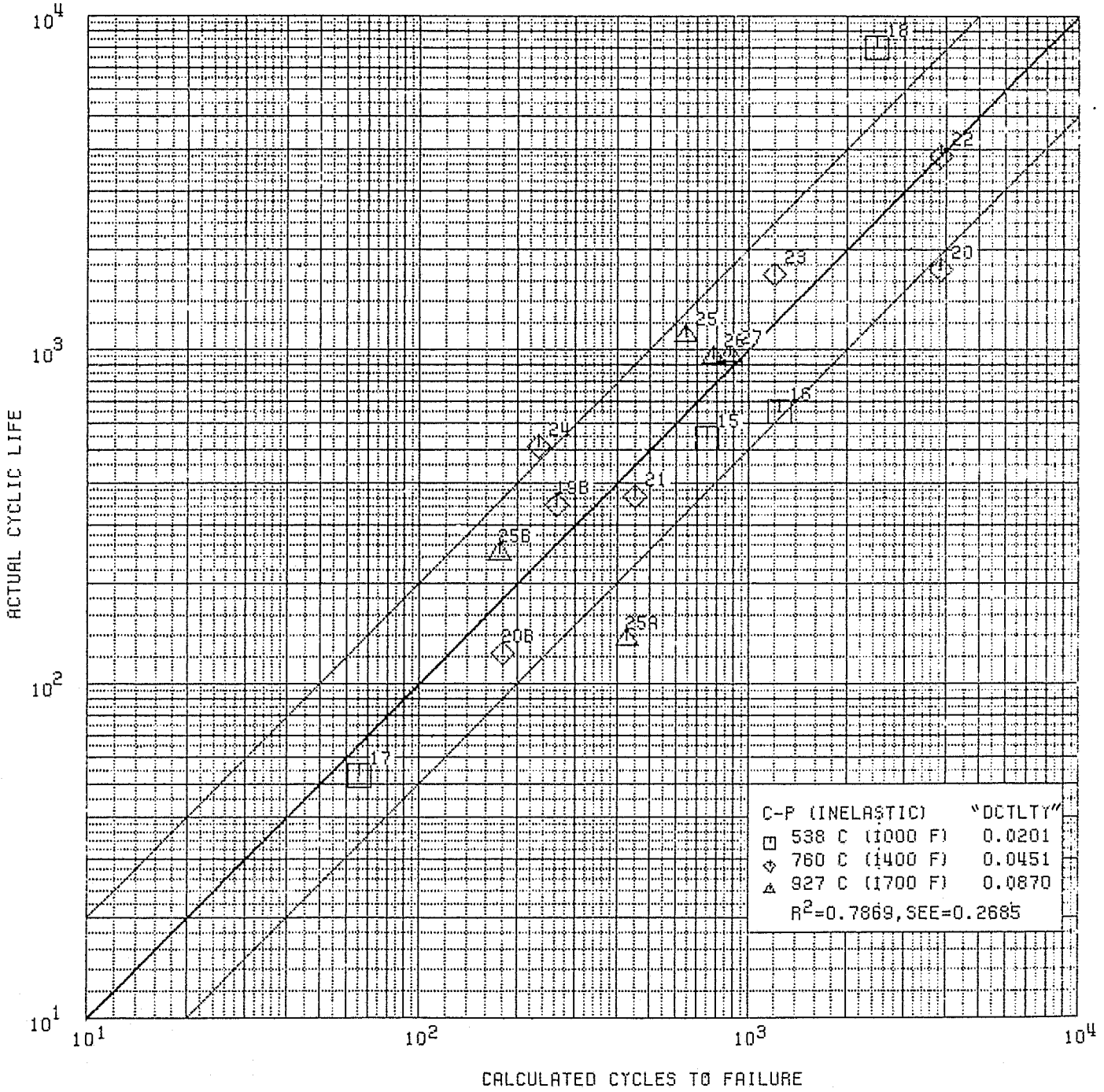

Figure 30. Actual vs Calculated Cyclic Life, for CP-Type Tests on CA-101

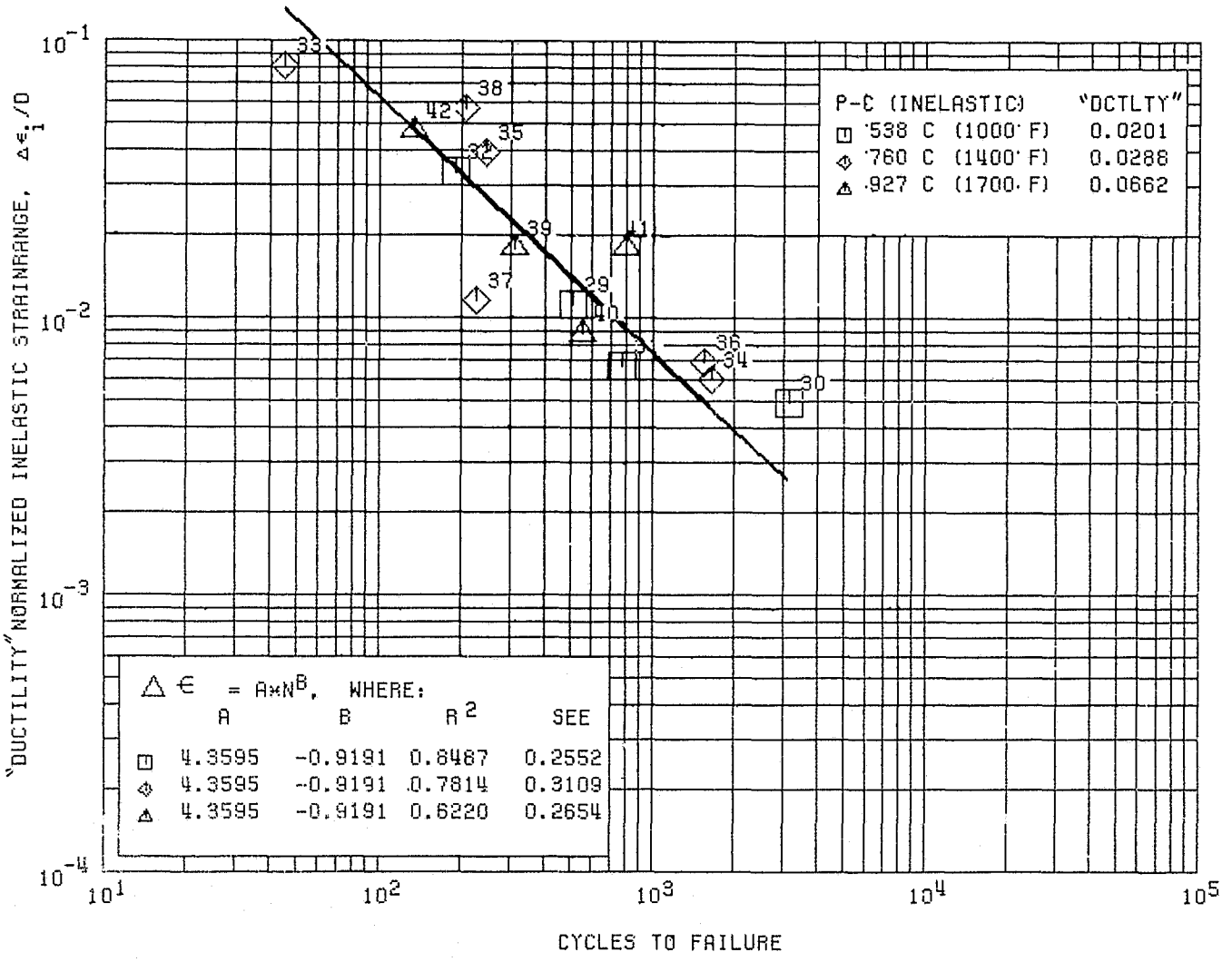

Figure 31. "Ductility" Normalized Inelastic Strainrange vs Cycles to Failure, for PC-Type Tests on CA-101

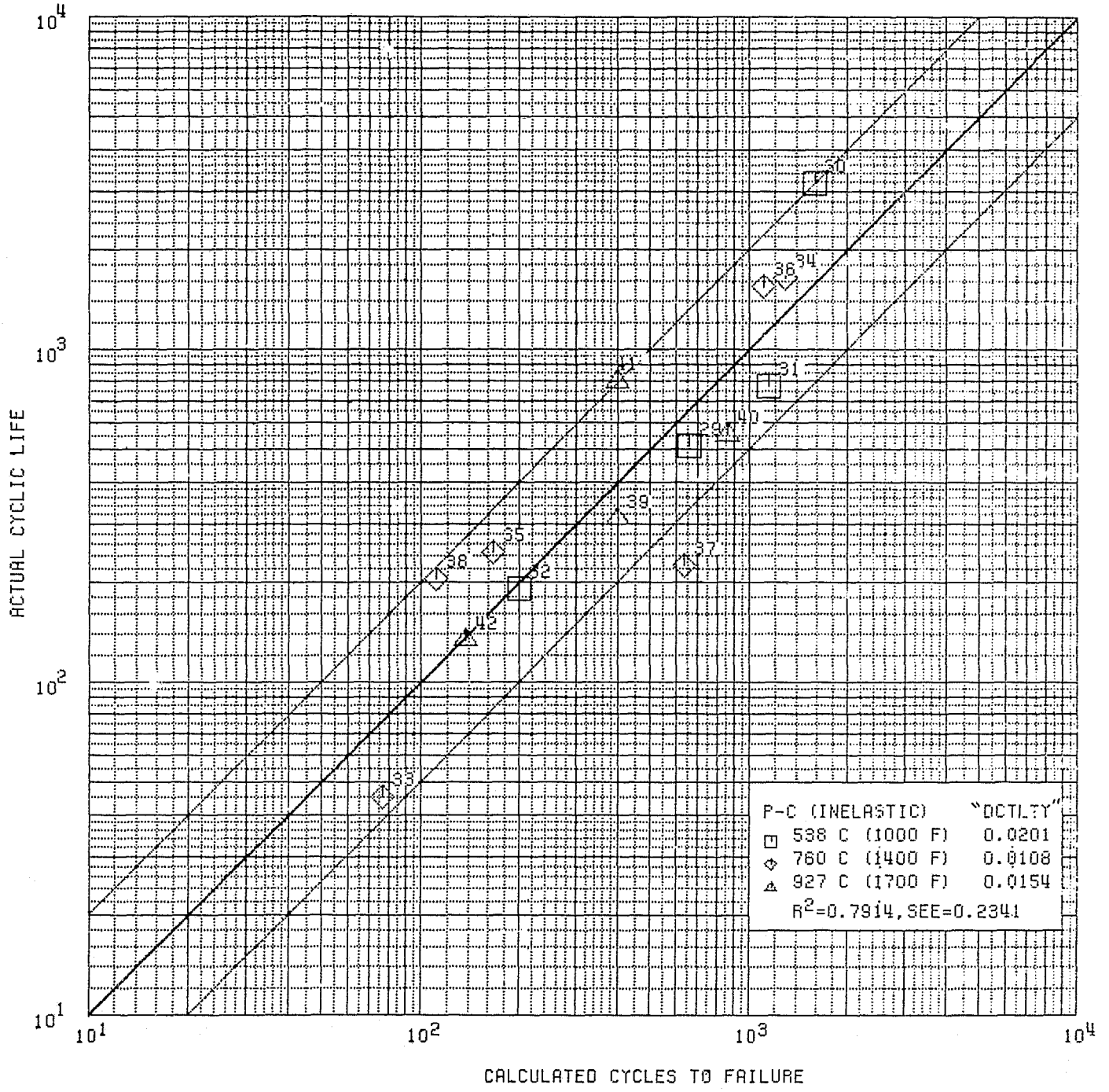

Figure 32. Actual vs Calculated Cyclic Life, for PC-Type Tests on CA-101

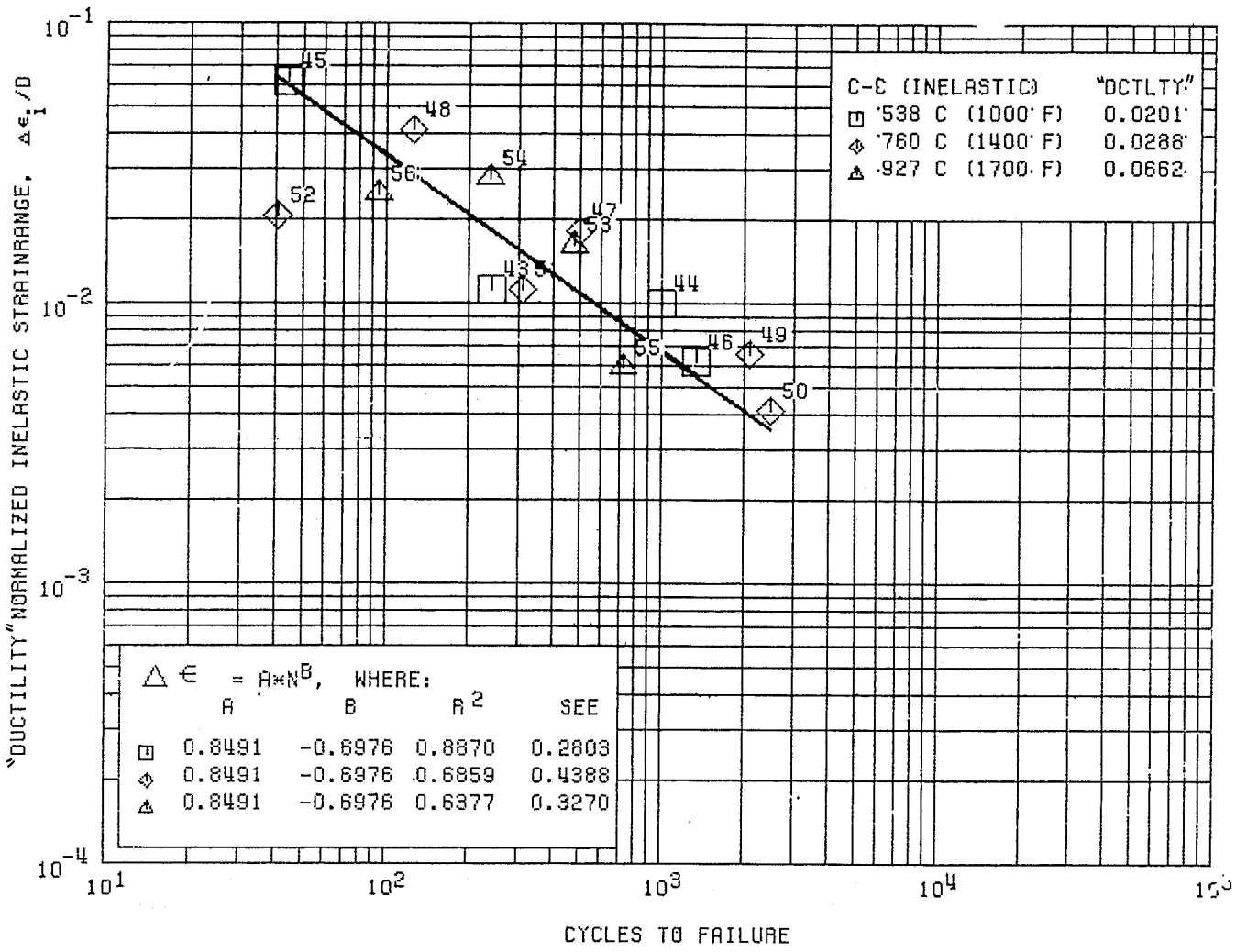

Figure 33. "Ductility" Normalized Inelastic Strainrange vs Cycles to Failure, for CC-Type Tests on CA-101

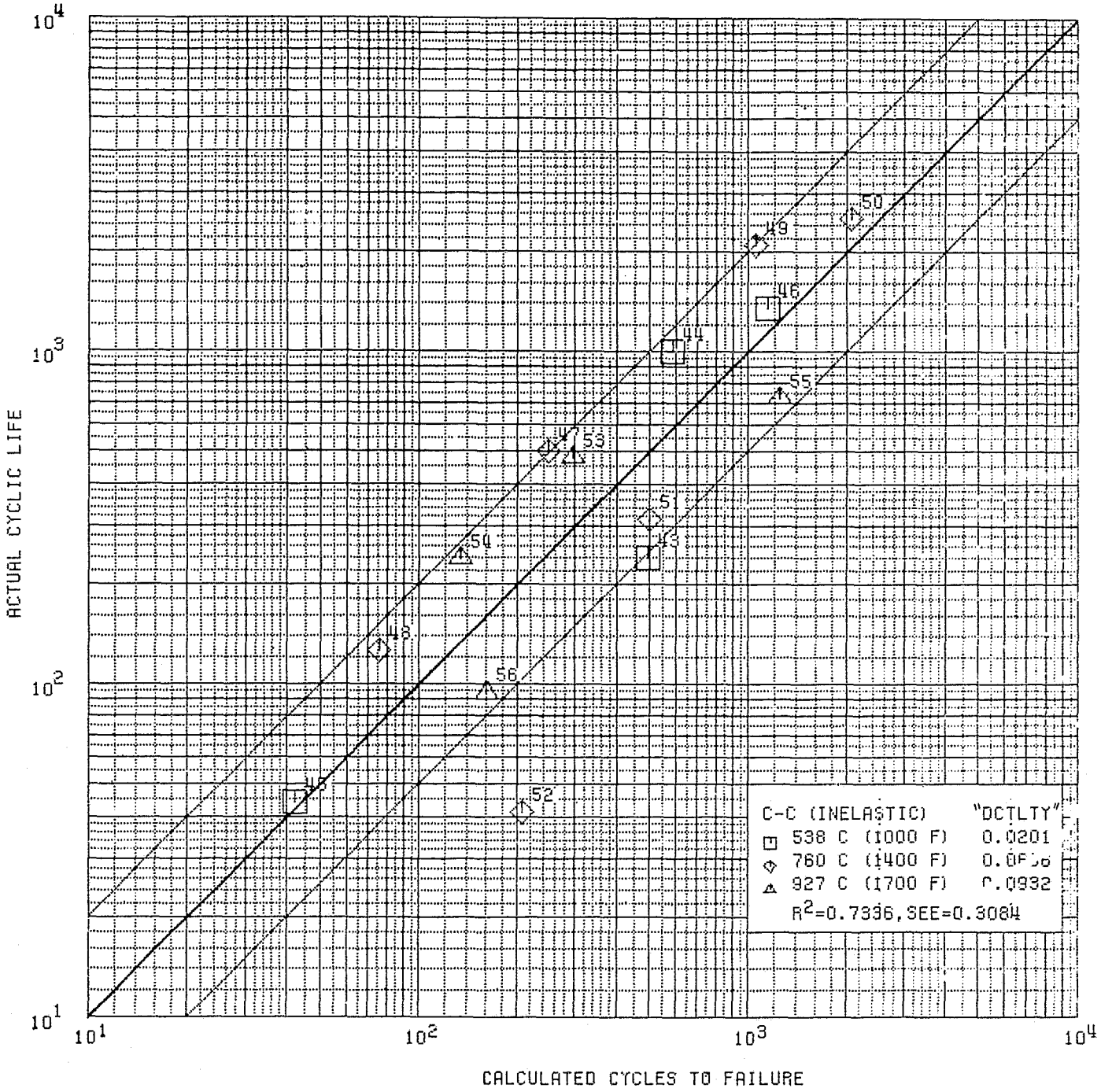

Figure 34. Actual vs Calculated Cyclic Life, for CC-Type Tests on CA-101

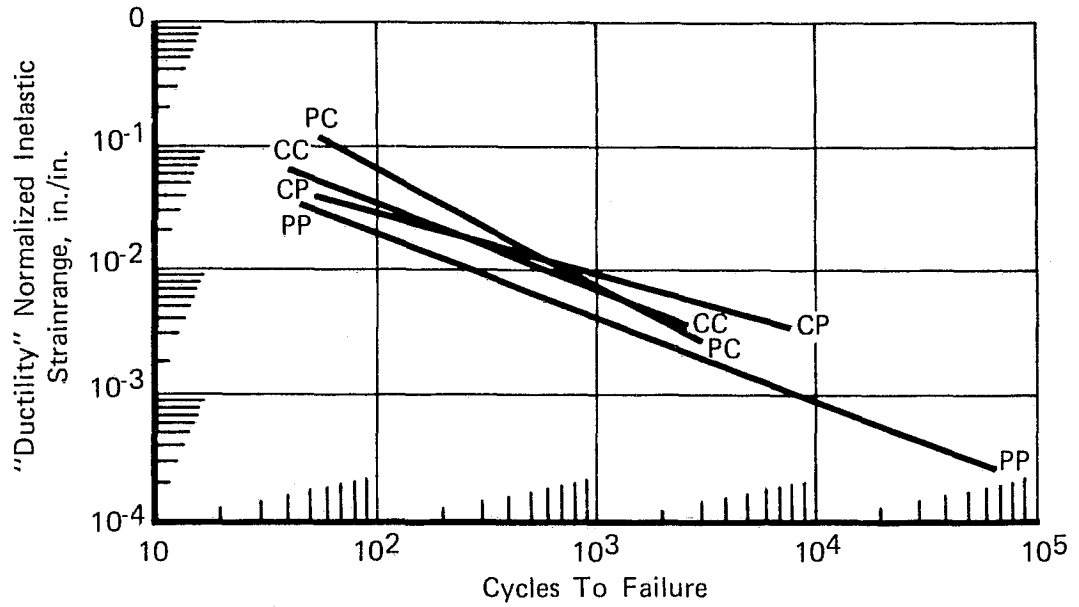

Figure 35. "Ductility" Normalized Inelastic Strainrange vs Cycles to Failure for CA-101 FD 97728

B. PRESENTATION AND EXPLANATION OF INCREMENTAL PARTITIONING RESULTS

The previous section presented the procedure used to "ductility" normalize the LCF test results. To use these results to predict cyclic life under the influence of some particular hysteresis loop, the constituent fraction (PP, PC or CP, CC) of that loop must be determined. The isothermal incremental partitioning procedure used to accomplish this is described in the following paragraphs.

1. Test Procedure and Rationale

For convenience, test IP-1 is used as an example. Test conditions, given in table VII were T = 927°C (1700°F), $\Delta\epsilon_{total}$ = 0.010 in./in., at 2 cycles per minute test frequency.

STEP 1 - The cyclically stable hysteresis loop to be partitioned (figure 36) is generated using the standard completely reversed, axial strain controlled test, during which the load-time history is monitored.

STEP 2 - The resulting load vs time relationship is then divided into 24 equal time increments and the load at the end of each time interval is recorded.

Table VI. Isothermal Incremental Partitioning Tests

Specimen	Temperature	Cycle Definition	Total Strainrange $\Delta \epsilon_{total}$ (in./in.)	Inelastic Strainrange $\Delta \epsilon_i$ (μin./in.)	Constitutive Fractions			
					PP	PC	CP	CC
IP-1	927°C (1700°F)	2 cpm	0.010	3330	0.015	0.090	None	0.895
IP-2	538°C (1000°F)	2 cpm	0.010	235	0.451	0.085	None	0.464
IP-3	927°C (1700°F)	2 cpm + 2 min T - dwell	0.010	3719	0.094	None	0.024	0.882
IP-4	538°C (1000°F)	2 cpm + 2 min T - dwell	0.010	243	0.358	0.078	None	0.564
IP-5	927°C (1700°F)	0.5 cpm	0.010	3400	0.097	None	0.079	0.824
IP-6	538°C (1000°F)	0.5 cpm	0.010	350	0.417	None	0.137	0.446
IP-7	927°C (1700°F)	2 cpm	0.006	1035	0.045	None	0.054	0.901
IP-8	538°C (1000°F)	2 cpm	0.006	50(1)	0.5	0.0	0.0	0.5
IP-9	538°C (1000°F)	2 cpm + 2 min C - dwell	0.010	344	0.137	0.084	None	0.779
IP-10	927°C (1700°F)	2 cpm + 2 min C - dwell	0.010	4212(2)	0.264	None	0.069	0.667
IP-11	760°C (1400°F)	2 cpm + 2 min T - dwell	0.010	405	0.049	0.136	None	0.815
IP-12	760°C (1400°F)	2 cpm	0.010	325	None	0.126	None	0.874
IP-13	760°C (1400°F)	5 cpm	0.010	375	None	0.216	None	0.784

(1) The inelastic strainrange (50μ) is too small to partition. Fractions are based on trends exhibited by IP-2, IP-4, and IP-6.

(2) Load controlled partitioning test ran between +0.8% and -0.34% strain because compressive set was partially relieved during change from strain to load control.

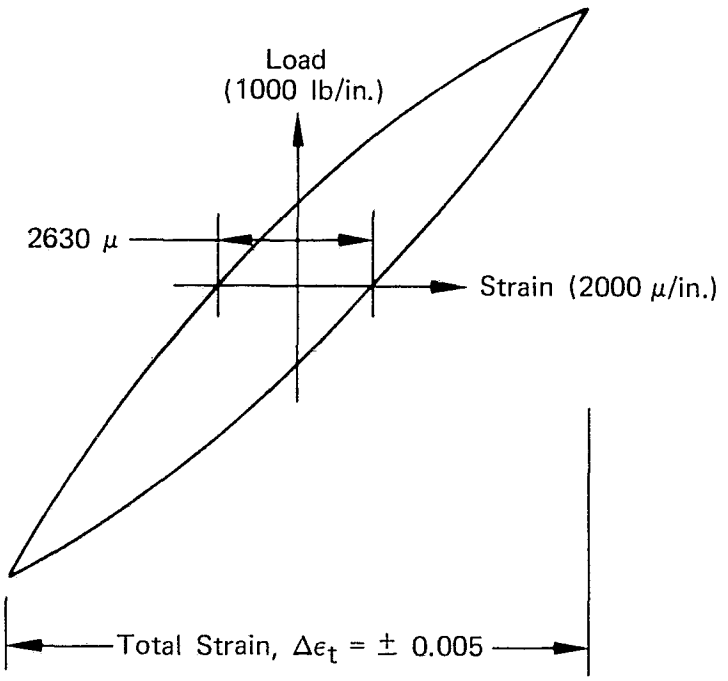

Figure 36. Load-Strain Hysteresis Loop, Test IP-1 FD 97729

STEP 3 - Next, the test is changed from strain to load control, and the end-point loads are applied very rapidly (0.1 sec) and then maintained for the duration of that time interval.

The test cyclic frequency remains constant and the partitioned loop nearly* coincides with the original loop at the end-points of each time interval shown in figure 37. Figure 38 schematically represents a portion of the load-strain-time history of the partitioned hysteresis loop, IP-1.

As can be seen in figure 38 the load varies in a stepwise manner but the resulting strain does not. The slope of the strain-time plot, over each of the 24 intervals, is the strainrate for that interval.

STEP 4 - To determine the time dependent strain, a plot is made of strainrate vs time for each half of the cycle, tension and compression (figures 39 and 40).

STEP 5 - The area under each curve represents the amount of creep (time dependent) strain during that half cycle.

---

*The average load during each interval of the partitioned loop is greater than the average load in the corresponding time interval of the original loop. In the partitioned loop, the incremental average load is nearly equal to the end-point load, but in the original loop the incremental average load is about half the end-point load.

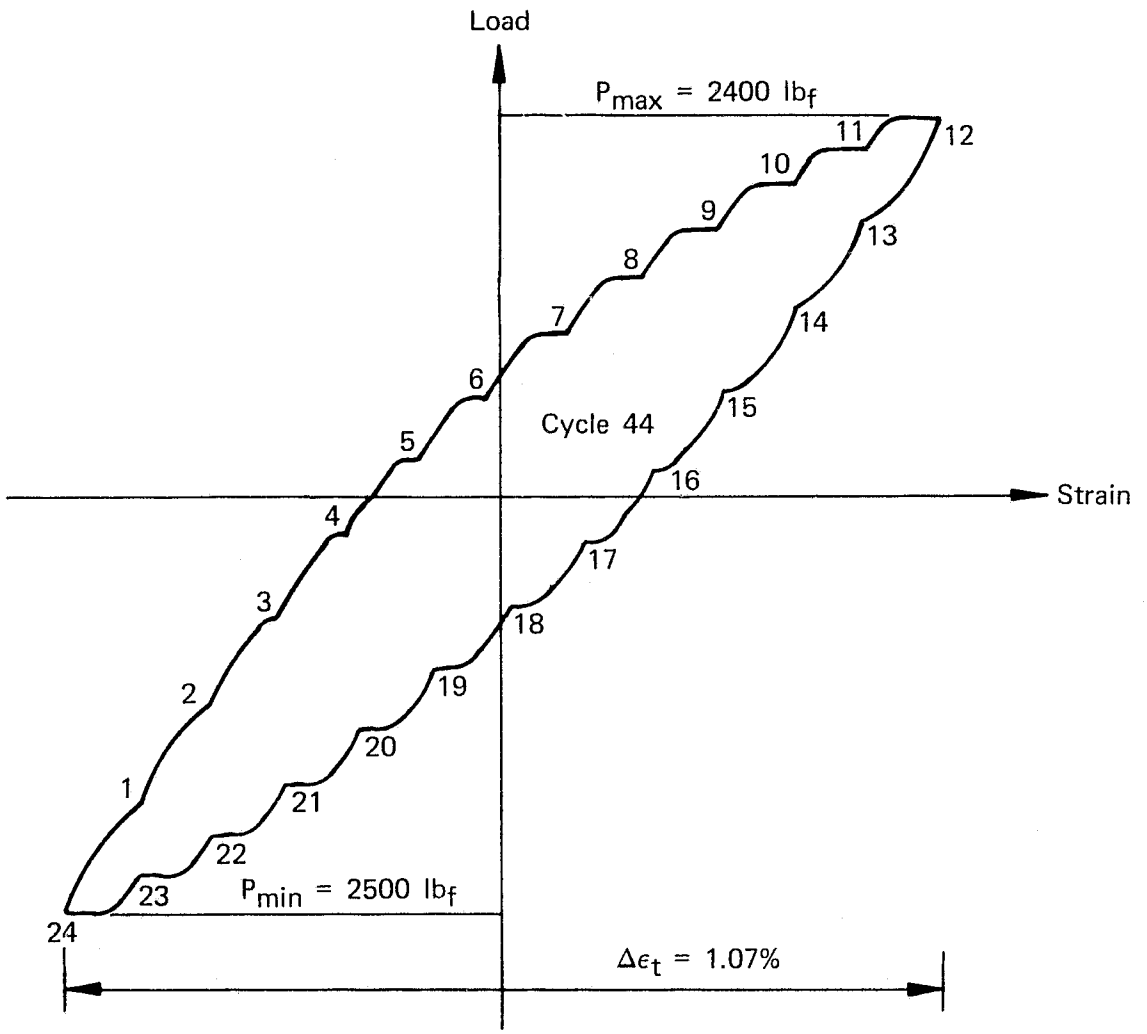

Figure 37. Partitioned Load-Strain Hysteresis Loop, Test IP-1 FD 97730

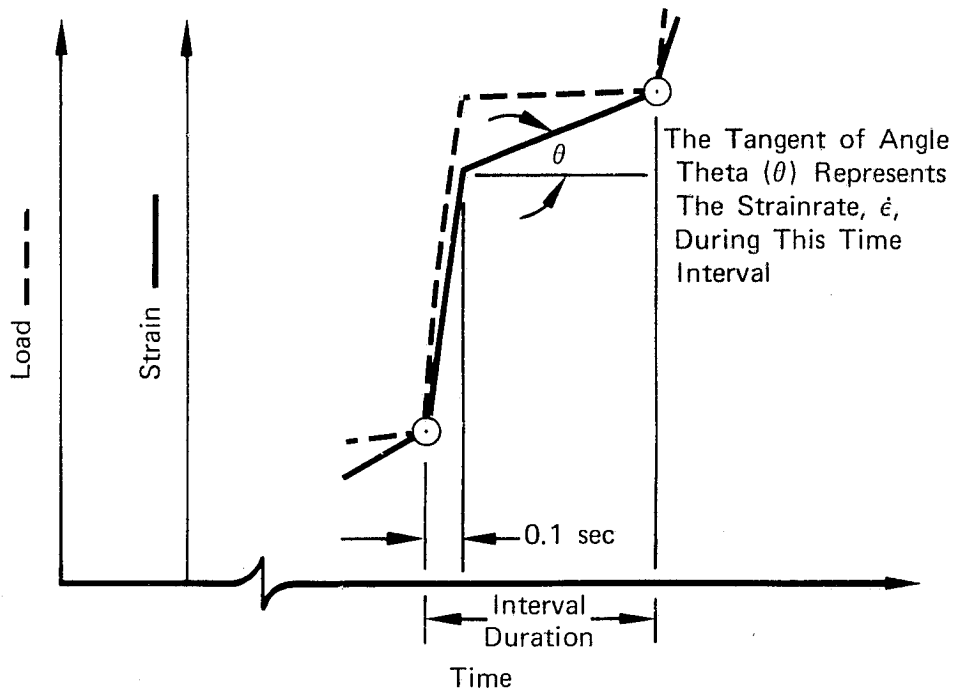

Figure 38. Schematic Representation of an Interval of Load-Strain-Time History FD 95930

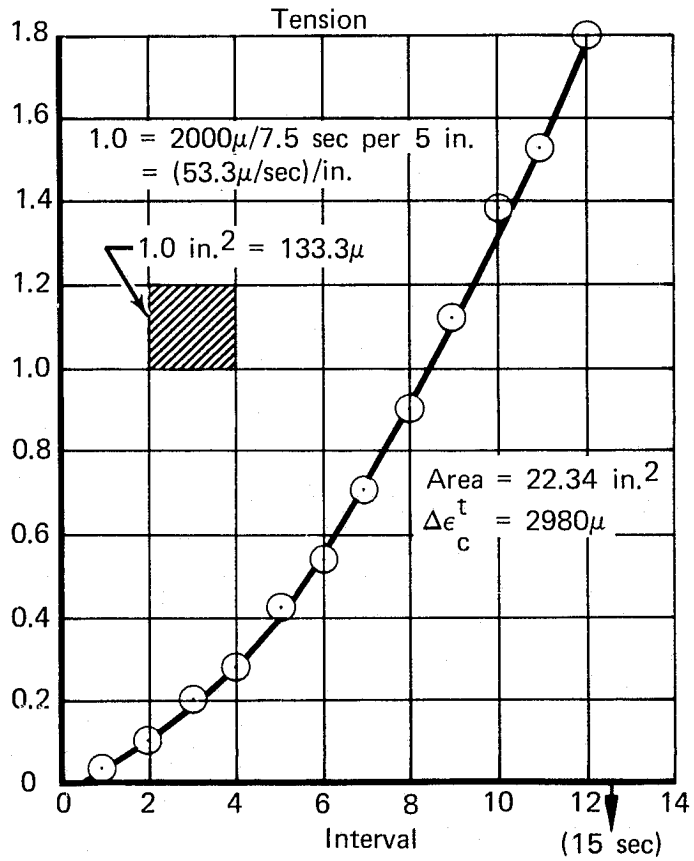

Figure 39. Strainrate vs Cycle Interval (Time) FD 97731

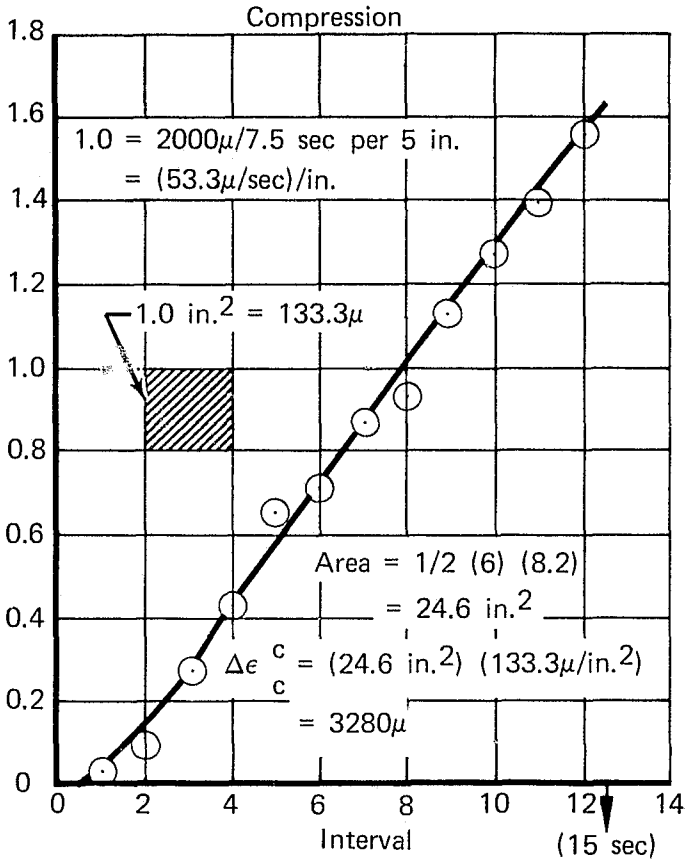

Figure 40. Strainrate vs Cycle Interval (Time) FD 97732

In this example, the total inelastic strain, $\Delta\epsilon_i = 3300\mu$, is comprised of 2630μ measured from the original loop (figure 37), plus 700μ necessary to account for the observed 7% increase in total strain during the load controlled cycle (figure 38) (1.0% to 1.07% total strain). This increased strain is expected because of the longer time-at-load (and therefore high incremental average load) during each time interval of the load controlled test.

Using the method outlined by Halford*, the constitutive fractions of PP, CC, and CP or PC are determined. The computation of these fractions is included here as an illustration of the procedure.

$\Delta\epsilon_i$ = 3330μ, total inelastic strain

$\Delta\epsilon_c^t$ = 2980μ, tension-creep (figure 39)

$\Delta\epsilon_c^c$ = 3280μ, compression-creep (figure 40) from which,

$\Delta\epsilon_p^t$ = $3330-2980 = 350\mu$, tension-plasticity

*Halford, G. R., and S. S. Manson, "Life Prediction of Thermal Mechanical Fatigue Using Strainrange Partitioning," NASA TM X-71829, November 1975.

$\Delta\epsilon_p^c$ = 3330-3280 = 50 μ, compression-plasticity

$\Delta\epsilon_{pc}$ = 3280-2980 = 300 μ.

The net inelastic components are,

$\Delta\epsilon_{pp}$ = 50 μ (smaller $\Delta\epsilon_p$)

$\Delta\epsilon_{cc}$ = 2980 μ (smaller $\Delta\epsilon_c$)

$\Delta\epsilon_{pc}$ = 300 μ (difference $\Delta\epsilon_c$ = difference $\Delta\epsilon_p$)

Finally, the strainrange fractions are calculated:

F_{pp} = 50/3330 = 0.015

F_{cc} = 2980/3330 = 0.895

F_{pc} = 300/3330 = 0.090

It is interesting to note the very small (1.5%) PP component in this low frequency (2 cpm), zero dwell test. This qualitative result has been inferred from the relative positions of the individual life lines which show PP lives to be shortest of the four basic cycle definitions (figure 35, Section V.A.2). This relationship could occur only if PP represented a small fraction of the damage done during CP, PC and CC cycle testing.

The disparity between computed PP-fractions of similar hysteresis loops, tests IP-1 and IP-5, (both at 927°C (1700°F) and ±0.005 in./in.; 2 cpm and 0.5 cpm, respectively) illustrates the inherent difficulty in any experiment in which computed values approach the resolution of the parameter being measured (e.g., strain). Experience here has indicated an approximate 40μ uncertainty in strains computed from measured parameters.

A final note on the incremental partitioning test procedure: a fundamental assumption of the methodology is that load can be applied as a step function (Δt = 0.1 sec) and then maintained as a constant for some successive time interval (e.g., Δt = 1.15 sec). In most cases this assumption is valid; however, those hysteresis loops displaying very little inelastic strain ($\Delta\epsilon_i < 100\mu$) demand special attention. The load-time relationship reveals that the load tends to increase in tension (decrease in compression) so that the observed increase (decrease) in strain is not entirely time dependent (creep) but has an elastic component produced by the slightly changing load ($\dot{P} < 15$ lb$_f$/sec) observed to occur during the load dwell.

2. Results and Conclusions

The test conditions and results of the isothermal incremental partitioning (IP) tests are presented in table VI.

The most remarkable result of the IP testing is the relatively small proportion of PP-type strain which was measured. In general, tests conducted at 927°C (1700°F) showed less than 10% PP-type strain even when tested using a sawtooth waveform, with no dwells. Although smaller than might have been expected, the magnitude of the measured PP constitutive fractions agrees well with other estimates of its effect (Sections IV.D.3.a, and V.C). Constitutive fractions of mixed cycles PC and CP were found to be similarly small. In these high temperature tests, CC-type strain predominates, accounting for between 80% and 90% of the inelastic strain.

As expected dwell tests exhibited greater creep strain than sister tests conducted with no dwell; however, the differences were not dramatic.

The lower temperature, 538°C (1000°F), tests showed much larger fractions of PP-type strain, as would be expected owing to ductility differences; however, the measured fractions, F_{pp}, were about 40% smaller than the nearly 100% anticipated. Again CC-type strain constituted the largest fraction of inelastic strain.

Intermediate temperature 760°C (1400°F) results fell between those of the higher and lower temperature, as expected. CC-type strain was the largest constitutive fraction.

C. INTERACTION DAMAGE RULES

Some type of damage rule is basic to the application of Strainrange Partitioning. The Interaction Damage Rule, and a proposed Alternative Rule will be discussed in detail here.

1. The Interaction Damage Rule

The Interaction Damage Rule is given by:

$$1/N_f = F_{pp}/N_{pp} + F_{pc}/N_{pc} + F_{cp}/N_{cp} + F_{cc}/N_{cc}$$

where:

N_f = cyclic life under some complex hysteresis loop

$F_{a,b}$ = constitutive fraction of type a,b inelastic strainrange contained in that hysteresis loop

and

$N_{a,b}$ = cyclic life expected were the entire inelastic strainrange of type a,b.

As was discussed earlier in Section IV. A, any real loop can contain, at most, three of these four constituents, so for simplicity the Rule may be written as:

$$1/N_f = \sum_{j=1}^{3} F_j/N_j \qquad \text{(Interaction Damage Rule)}$$

This Rule can be seen to be a special case of a more general cumulative damage rule:

$$N_f^n = \sum_{j=1}^{3} F_j N_j^n, \quad -1 \leq n \leq +1^* \qquad \text{(General Rule)}$$

2. An Alternative Rule

To provide a basis for comparison, an alternative rule where n = +1, will be investigated. This rule can be written as:

$$N = \sum_{j=1}^{3} F_j N_j \qquad \text{(Alternative Rule)}$$

For illustrative purposes consider a hypothetical case where only two types of damage are present, and both in equal proportions, i.e., $F_1 = F_2 = 0.5$. Since it is not uncommon to observe an order of magnitude difference in life between the shortest and longest cycle definition, suppose also that $N_2 = 10N_1$.

Now compare the cyclic life computed using these two rules (n = -1) and (n = +1).

Using The Interaction Damage Rule

$$\begin{aligned} 1/N_f &= 0.5/N_1 + 0.5/N_2 \\ &= 0.5/N_1 + 0.5/10N_1 \\ &= (0.5 + 0.05)/N_1 \\ N_f &= (1/0.55)N_1 = 1.818N_1 \end{aligned}$$

Whereas an Alternative Rule would give:

$$\begin{aligned} N_f &= 0.5N_1 + 0.5N_2 \\ &= 0.5N_1 + 0.5(10N_1) \\ &= (0.5 + 5.0)N_1 \\ &= 5.5N_1 \end{aligned}$$

---

*n could be any real number but is limited here for simplicity.

From this it can be seen that The Interaction Damage Rule favors the shorter life in this 50% type 1, 50% type 2 hypothetical case, and the Alternative Rule favors the longer life. Of course, the minimum value expected in either case is N_1, and the maximum value, N_2. Both results are bounded by these numbers.

Figure 41 compares these two rules for cases where N_2 is some other multiple of N_1. From this, an interesting conclusion can be drawn: The Interaction Damage Rule is asymptotic. That is, even if the other contributing lives were infinite, the maximum value possible for life computed using the Rule equals the shortest contributing life (PP, PC, CP or CC) times the inverse of its constitutive fraction.

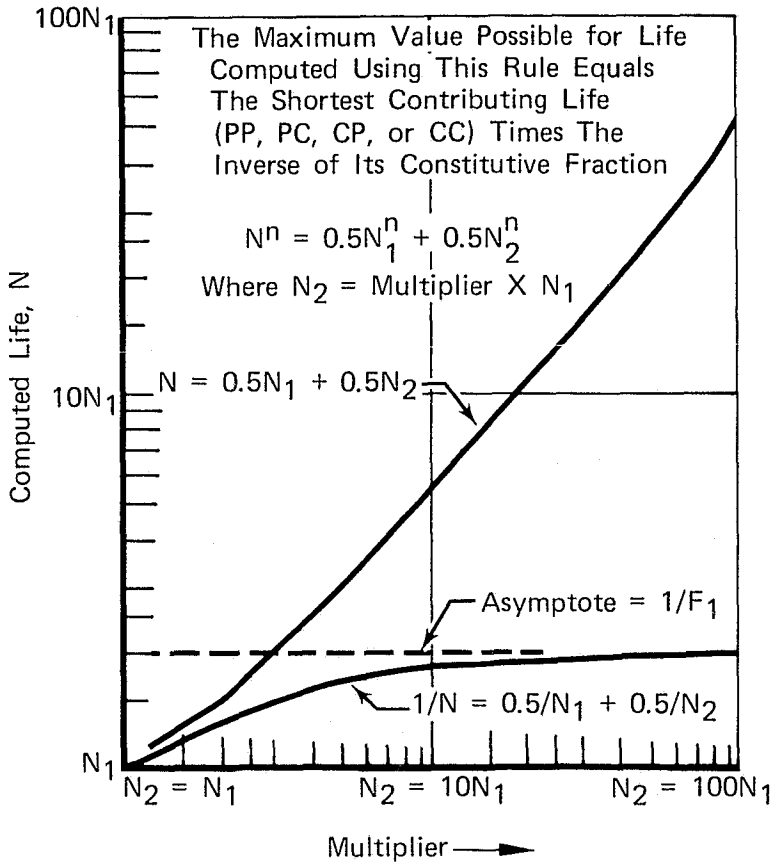

Figure 41. The Interaction Damage Rule Is Asymptotic FD 95617

This observation substantiates the conclusion made earlier (Section IV.D.3.a) that PP components are negligible in the other three basic tests, PC, CP, and CC. For if the Interaction Damage Rule is applicable* to this material, under these testing conditions, then PP components can exist only to a negligible degree or computations using the Rule result in negative values for N_f.

*Section V.D.2 will show The Interaction Damage Rule proved satisfactory in predicting upper and lower bounds on thermal-mechanical cyclic life.

Values actually measured for PP components during the incremental partitioning (IP) portion of the program were found to be smaller than what might have been expected (Section V. C. 2).

D. LIFE PREDICTION OF SPECIAL THERMAL-MECHANICAL LCF TESTS

To accomplish the thermal-mechanical tests, special testing hardware and special data analysis procedures were required, and are described here.

1. TMSC Test and MTS Equipment Capability

Thermal-mechanical, strain-cycling fatigue tests can simulate the important aspects of an actual thermal-strain fatigue cycle encountered by a turbine disk and blades in an automotive gas turbine engine cycle. Six axially loaded completely reversed strain-controlled tests were performed to vary in-phase and/or out-of-phase with one another. Results of the six tests are summarized in table VII.

A universal, computer-controlled closed-loop test system was used for all incremental partitioning and special low-cycle fatigue tests. The unit consists of two computer-controlled servo-systems; the one for the hydraulic system is capable of closed-loop control on load, strain, or displacement; the other is capable of closed-loop control on temperature. This equipment is shown in figure 42.

To provide system supervision of the test a processor unit is used combining a computer and teleprinter with an interface unit that monitors and commands various functions of the system. The computer is a Digital Equipment Corporation Model PDP8/L having 4K of internal core memory and a 1.6 sec cycle time. The computer uses fixed word lengths of 12 bits. Since one of the computer's main functions is to manipulate the converted analog data, 12 bits give more than enough resolution to ensure that none of the accuracy is lost. This computer is tied into the system using an interface unit. In the interface there are digital-to-analog converters. These converters provide signals that serve as commands to the servo-controller. The data for use by the computer are gathered by a high-speed multiplexer and converted at a rate up to 15,000 point/sec. To give real-time function to the system, a programmable clock and interrupt system are included.

All heating and cooling is accomplished using closed-loop servo-control. The command signal is supplied from the PDP8/L computer, while the feedback signal is supplied from a thermocouple with a 10-kw LEPEL power source induction heater phased with a pressurized cooling system. This closed-loop temperature system has an accuracy within ±2% over a range of 24°C to 1093°C (75°F to 2000°F) and has operated at temperature rates in excess of 110°C (200°F) per second in this range.

Table VII. Special Low-Cycle Fatigue Test Matrix

Specimen Ident.	Temperature Range (Phase With Strain)[1]	Total Mechanical Strainrange, in./in.	Inelastic Strainrange, μin./in.	Cyclic Frequency	Life Prediction[3] 538°C (1000°F)	Life Prediction[3] 927°C (1700°F)	Actual Life[4]
TM-1	538°C (1000°F) ⟷ 927°C (1700°F) in-phase	0.006	50	2 cpm	2997*	451	3790
TM-2	538°C (1000°F) ⟷ 927°C (1700°F) in-phase	0.010	300	2 cpm	321*	73	703
TM-3	538°C (1000°F) ⟷ 927°C (1700°F) out-of-phase	0.010	100	2 cpm	321*	73	250
TM-4	538°C (1000°F) ⟷ 927°C (1700°F) in-phase	0.007	250	2-min dwell[2] (tension only)	549*	106	532
TM-5	538°C (1000°F) ⟷ 927°C (1700°F) in-phase	0.010	450	0.5 cpm	182*	70	101
TM-6	538°C (1000°F) ⟷ 927°C (1700°F) out-of-phase	0.010	700	0.5 cpm	182	70*	46

[1] Tests 180 deg out-of-phase.

[2] 2 cpm ramp rate

[3] Value selected*

[4] Tests TM-3, TM-4, TM-5, and TM-6 were subjected to several Incremental Partitioning cycles. Actual life includes these load controlled cycles.

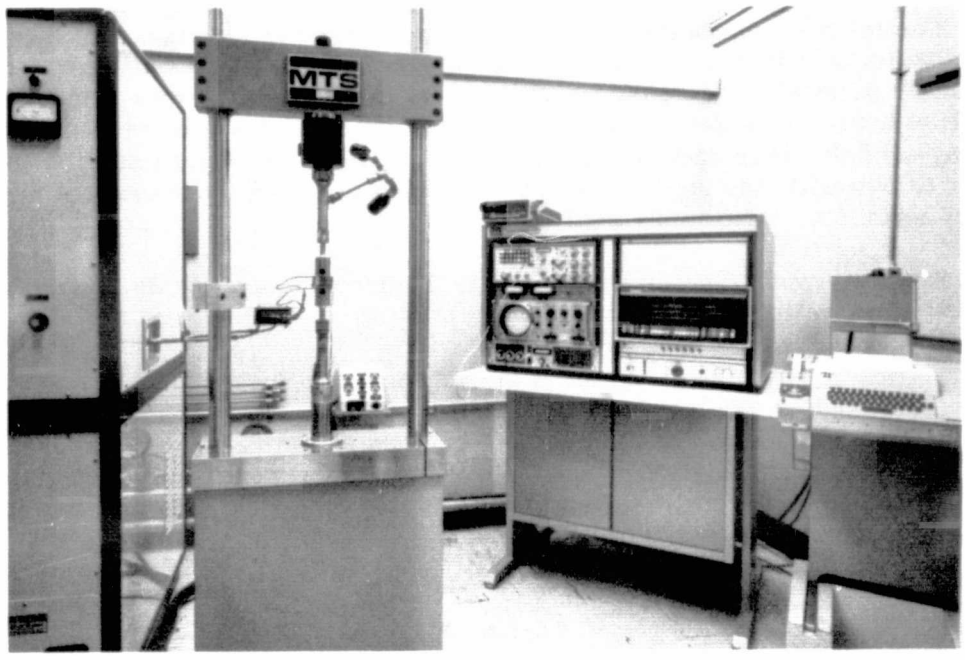

Figure 42. Computer-Controlled, Closed-Loop Test System FC 26560

Use of the computer allows continuous linear or nonlinear functions of strain and temperature vs time to be programed and used to control the test parameters. The testing equipment compensates for the thermal-free expansion strain by subjecting the specimen, extensometer clamps, and grips to the temperature vs time portion of the programed waveform. By holding the load at zero and measuring the strain at each data point defined on the waveform the free expansion strain can be determined and stored in the computer memory. As the test cycle is being performed, the free-expansion strain is being taken from memory for each point and is algebraically combined with the input total strain at that point to induce the desired total mechanical strain on the specimen.

The cycle used for this testing consisted of a modified sawtooth shape. This cycle is divided into 24 segments of time each with a corresponding temperature and strain. Use of the computer provides the capabilities of varying the functions of temperature with the strain. The computer generates a command signal to the temperature and strain servo-controllers on the basis of the input temperature and strain waveform. The thermal-mechanical cycle will not proceed from segment-to-segment until the computer has verified, via the temperature and strain feedbacks, that the specimen has responded as commanded; therefore, strain and temperature will have the desired phase relationship. Should these parameters not be maintained as commanded, with the error tolerance programmed, the system will shut down.

The total (mechanical plus thermal) strain and stress vs time was recorded on a dual-pen strip chart recorder at periodic cyclic increments. In addition, the time, mechanical strain, temperature, strain and temperature errors, and stress were also printed out via teletype at the desired cyclic increments, either programmed or upon command.

The tests were conducted using the same type of specimen as those used in the basic LCF tests. Induction heating was employed. Cooling was accomplished by several compressed airflow jets. When cooling was required the induction heater shut down and the computer triggered a solenoid valve controlling airflow, thus cooling the specimen. The servo-loop used the induction heater to override the cooling effect, reducing any cooling overshoot and ensuring a smooth, continuous cooling rate.

2. Strainrange Partitioning Applied to Thermal-Mechanical Strain Cycling Tests

To predict cyclic life of the TMSC tests it was necessary to use the results of the isothermal incremental partitioning (IP) tests presented in table VI. Actual incremental partitioning of the TMSC tests was attempted using the procedure described in Section V.B; however, the material response to the attempted temperature incrementation was disappointing, and made incremental partitioning of these nonisothermal tests impossible.

a. Prediction Procedure

The procedure used to predict the TMSC lives was first to compute the maximum and minimum expected life assuming isothermal conditions at both extremes of temperature. A choice was then made as to which of the two extremes would better represent the actual TMSC hysteresis loop, and as such would provide the life prediction* for that test.

To compute these extremes of life, the IP tests conducted at the maximum and minimum temperatures (927°C = 1700°F and 538°C = 1000°F) were used to provide the constitutive fractions necessary for use in The Interaction Damage Rule calculations.

The numerical analysis of specimen TM-1 provides an example of the computational procedure used to determine the upper and lower bounds on cyclic life.

Specimen TM-1 was cycled at 2 cpm between 538°C (1000°F) and 927°C (1700°F) with strain in-phase with temperature, reaching its maximum mechanical strain of + 0.003 in./in. at 927°C and minimum mechanical strain of -0.003 in./in. at 538°C.

Isothermal incremental partitioning tests IP-8 at 538°C (1000°F) and IP-7 at 927°C (1700°F) were used to compute the maximum and minimum life to be expected from specimen TM-1. Both tests IP-8 and IP-7 were at strain amplitudes of ±0.003 as was the thermal-mechanical test TM-1.

---

*The imprecision of this method of prediction and possible improvements are discussed in Section VII.

Calculations for the lower temperature life estimate; IP-8:

$\Delta\epsilon_i = 50\,\mu$ in./in. and,

Inelastic Strain Type	PP	PC	CP	CC
Constitutive Fraction (table VI)	0.5	0	0	0.5
Normalizing "Ductility" (Figures 27, 29, 31, and 33)	0.02			0.02
$\Delta\epsilon_i/D$	2.5×10^{-3}			2.5×10^{-3}
N_f (figure 35)	2300			4300

Using The Interaction Damage Rule:

$$1/N = F_{pp}/N_{pp} + F_{pc}/N_{pc} + F_{cp}/N_{cp} + F_{cc}/N_{cc}$$

$$1/N = 0.5/2300 + 0 + 0 + 0.5/4300 \longrightarrow N = 2997$$

And calculations for the higher temperature, IP-7:

$\Delta\epsilon_i = 1035$ and,

Inelastic Strain Type	PP	PC	CP	CC
Constitutive Fraction (Table VI)	0.045	0	0.54	0.901
Normalizing "Ductility" (Figures 27, 29, 31, and 33)	0.0662		0.0870	0.0932
$\Delta\epsilon_i/D$	1.56×10^{-2}		1.19×10^{-2}	1.11×10^{-2}
N_f (Figure 35)	150		460	500

Using the Interaction Damage Rule:

$$1/N = 0.045/150 + 0 + 0.054/460 + 0.901/500 \longrightarrow N = 451$$

Now, it remains to select one of these two bounding lives, either 2997 or 451, as the prediction for specimen TM-1.

Figure 43 presents the load-mechanical strain cycle experienced by specimen TM-1. The very small inelastic strainrange, $\Delta\epsilon_i = 50\mu$ in./in., exhibited during this temperature in-phase with strain test, is more closely represented by that measured during IP-8 ($\Delta\epsilon_i = 50\,\mu$in./in.) than by IP-7 ($\Delta\epsilon_i = 1035\,\mu$in./in.). Therefore, the life prediction for test TM-1 is 2997, the life calculated assuming constitutive fractions measured during incremental partitioning test IP-8.

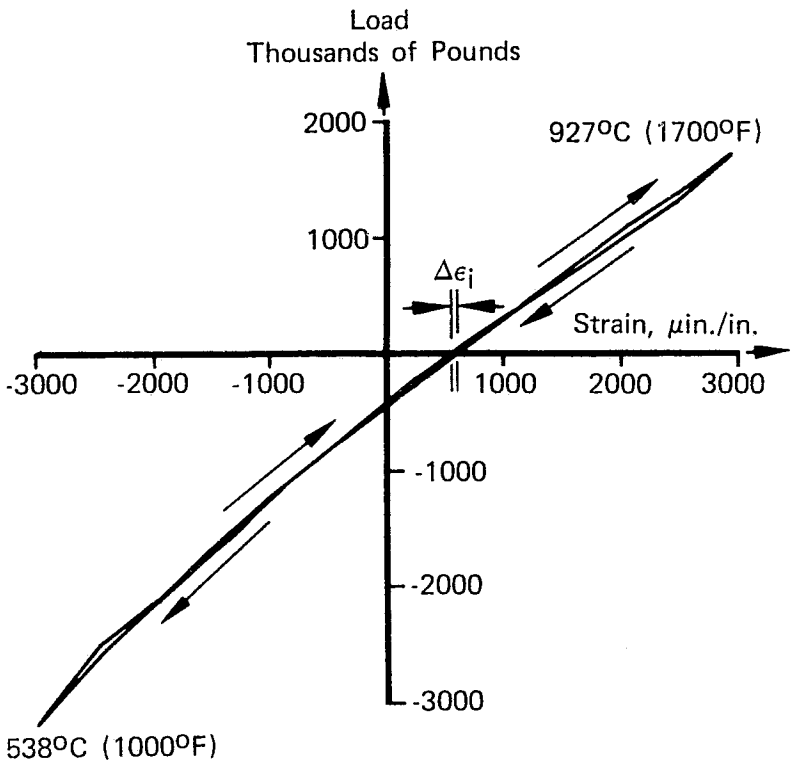

Figure 43. Load-Mechanical Strain Behavior of Thermal-Mechanical Strain Cycling Test TM-1, $\Delta\epsilon_t = 0.006$ Temperature In-Phase With Load

FD 97733

A procedure similar to that illustrated for test TM-1 was followed for the other TMSC tests. The inelastic mechanical strainrange measured for each test was used to select which of the two limiting cases more closely represented the particular TMSC test and as such provided the life prediction for that test. Test TM-4 required one further calculation. Because the reference incremental partitioning tests, IP-4 and IP-3 were tested at 1% total strainrange, and test TM-4 was at 0.7%, the reference inelastic strainranges were multiplied by 0.7/1.0 prior to life calculations using The Interaction Damage Rule.

Table VII presents the results of the TMSC tests.

Figure 44 compares the thermal-mechanical predictions with the actual cyclic lives. As can be seen, all predictions were within a factor of ±2 of the observed cycles to failure. Since this was the same range of data scatter observed in the four basic LCF tests, the TMSC predictions are felt to be as accurate as could be expected.

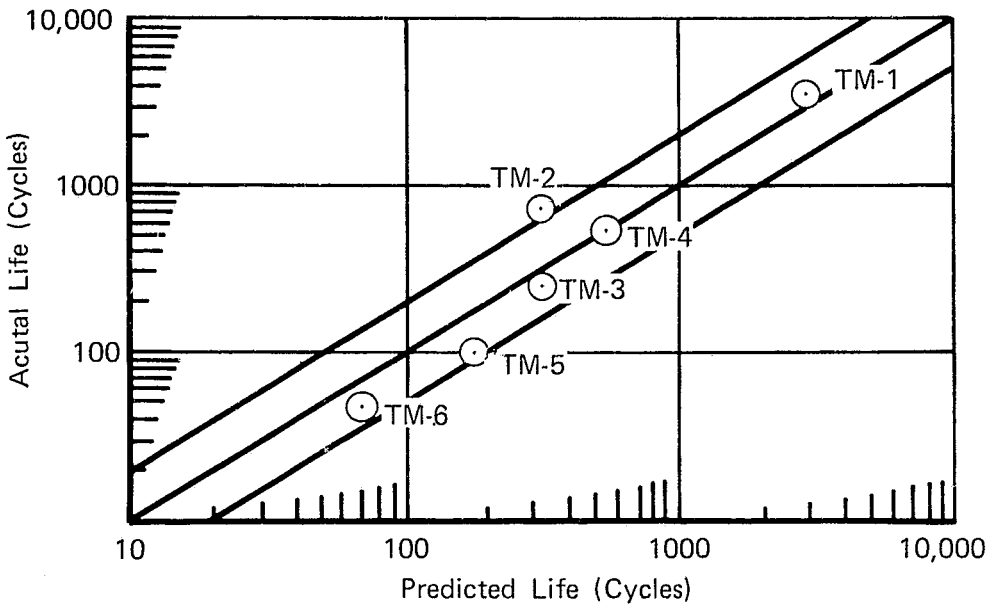

Figure 44. Thermal Mechanical Life Predictions Agree With Actual Cyclic Lives Within a Factor of ±2 FD 97734

b. Effects of Mean Stress

In retrospect, the difference observed in the in-phase and out-of-phase cyclic lives can be explained in terms of mean operating stress. Investigation of the stress-time relationship in test TM-2 (in-phase) shows an initial mean load of -3.78 kN (-850 lb_f). The greater ductility at 927°C (1700°F) required a smaller tensile load than the reversing compressive load, which was applied at lower 538°C (1000°F) temperature (ductility). In addition to operating under a compressive mean stress, TM-2 also exhibited stress relaxation throughout the entire test, resulting in a continually decreasing maximum tensile load. The specimen ran 703 cycles.

By comparison, test TM-3 (out-of-phase) showed an initial mean load of +2.89 kN (+650 lb_f), and furthermore this tensile mean stress was not allowed to relax, because of the low ductility at maximum tensile stress. The cyclic life of TM-3 was 250 cycles, only about a third of the life demonstrated by its in-phase sister, TM-2.

Scrutiny of sister tests TM-5 and TM-6 showed similar behavior. The in-phase test TM-5 ran at -3.56 kN (-800 lb_f) initial load and exhibited stress relaxation throughout its life of 101 cycles. Out-of-phase test TM-6, ran at +3.11 kN (+700 lb_f) initial load and failed after 46 cycles, experiencing no stress relaxation.

c. Fracture Analysis

Figures 45 through 47 present scanning electron micrographs of specimens TM-1, TM-2, TM-3, and TM-4, respectively. The fracture mode is predominately transgranular. Scanning electron micrographs for specimens TM-5 and TM-6 (figures 48 and 49) reveal mixed mode fracture. These results suggest that as this alloy is tested at frequencies representative of engine disk applications, the fracture modes behave as expected, that is, as temperature is increased and/or frequency decreased, the amount of intergranular fracture increases.

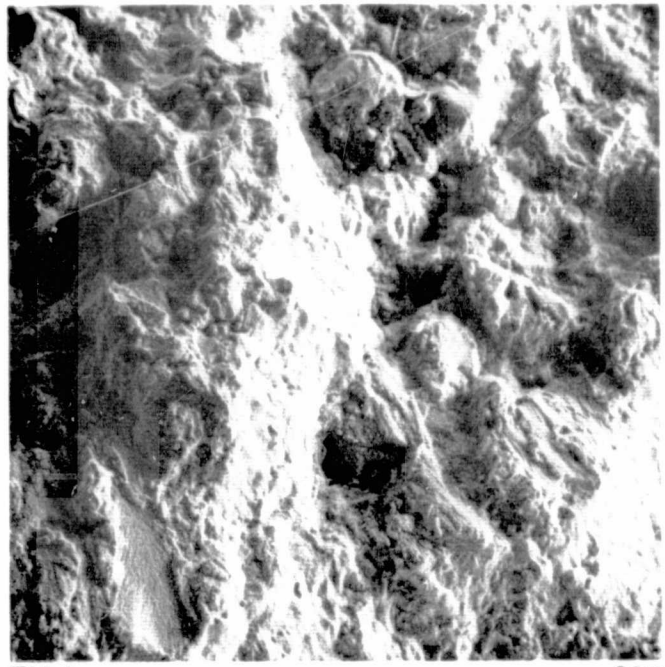

Figure 45. Scanning Electron Micrograph of Specimen TM-1 Indicating Transgranular Fracture at the Origin FD 95931

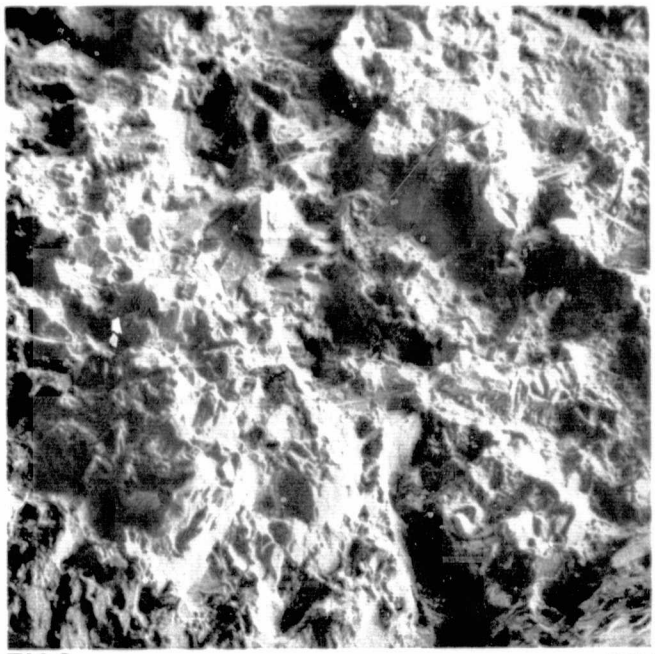

Figure 46. Scanning Electron Micrograph of Specimen TM-2 Indicating Transgranular Fracture at the Origin FD 95932

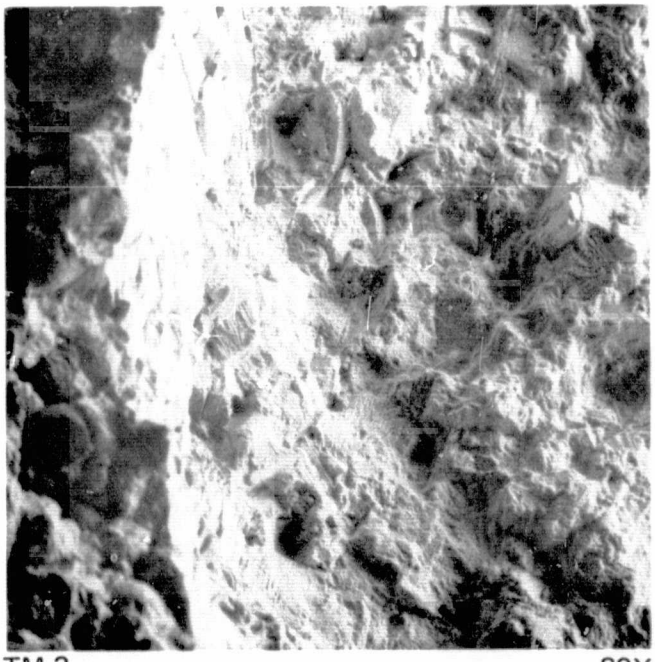

Figure 47. Scanning Electron Micrograph of Specimen TM-3 Indicating Cleavage and Transgranular Fracture at the Origin FD 95918

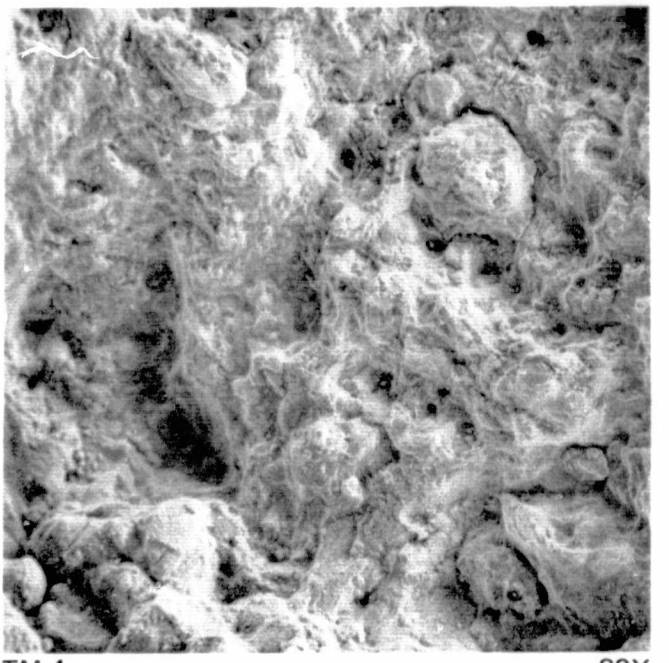

Figure 48. Scanning Electron Micrograph of Specimen TM-4 Indicating Transgranular Fracture at the Origin FD 95919

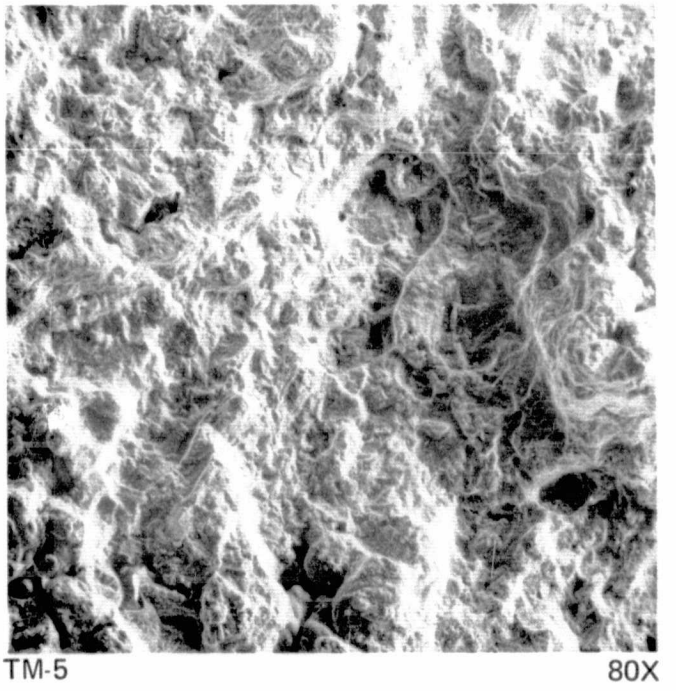

Figure 49. Scanning Electron Micrograph of Specimen TM-5 Indicating Mixed Mode Fracture at the Origin FD 95920

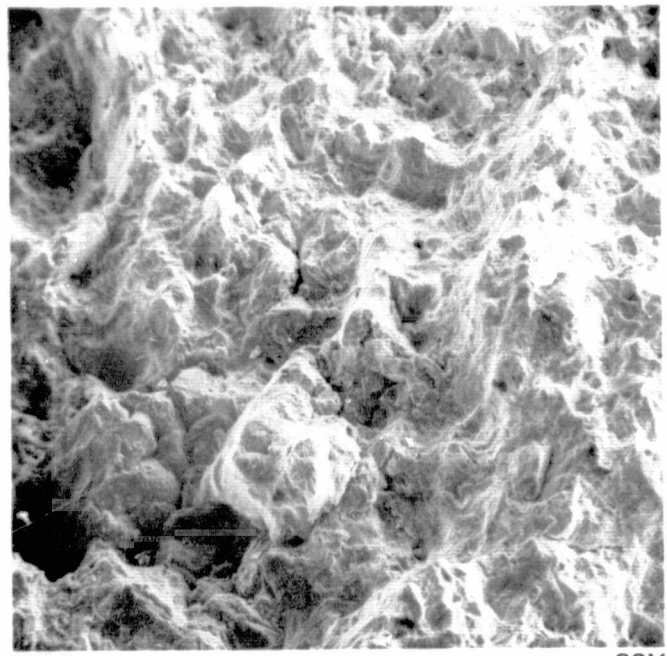

Figure 50. Scanning Electron Micrograph of Specimen TM-6 Indicating Mixed Mode Fracture at the Origin FD 95921

SECTION VI
RESULTS AND CONCLUSIONS

This section recalls the salient features of this program. References to the sections in which a particular topic was addressed are given parenthetically.

1. Strainrange Partitioning is a viable life prediction analysis procedure that was successful in predicting specimen life under complex thermal-mechanical strain cycling to within a factor of ±2, the same data scatter observed in the basic LCF tests (Section V.D.3).

2. CA-101, and in particular the casting of Heat 140B3429 used in this program, exhibited very low ductilities, resulting in small measured inelastic strainranges (Section III.C and IV.D).

3. For a given inelastic strainrange, PP-type test cycles exhibited shorter cyclic lives than test cycles containing strain dwells, PC, CP, or CC (Section IV.D.3.b).

4. The imposition of strain dwells has a salutory effect on specimen life, for CA-101 at approximately 1% total strain, between 538°C and 937°C (1000°F and 1700°F).

5. The PP component of the other three generic test types (PC, CP, and CC) is negligible for this material, under these test conditions (Section IV.D.3.a, Section V.B, and Section IV.C).

6. The incremental partitioning methodology developed here permits separation in real time of the plastic and creep components of inelastic strainrange (Section V.B.1).

7. The Interaction Damage Rule is asymptotic and so may affect conclusions drawn from calculations containing small values for any constitutive fraction (Section V.C.2).

8. Special statistical procedures were necessary to achieve "ductility" normalization (Section V.A.1).

SECTION VII
SUGGESTIONS FOR FURTHER STUDY (STRAIN DWELL VS STRESS DWELL)

An area suggested for further investigation is a quantitative differentiation between the effects of strain dwell, as used in this program, and stress dwell, a proposed alternative. Figure 51 illustrates these two dwell types, each conducted at the same total strainrange. The hysteresis loop containing strain dwell b-c can be seen to operate at a higher mean stress than a loop experiencing a stress dwell a-c. Higher σ_{mean} has a detrimental effect on cyclic life, but stress relaxation has been shown to have a beneficial effect on life (Section V.D.3.c). The cumulative result of these opposing effects experienced with strain dwell, should be investigated, and compared empirically and metallurgically, with results of stress dwell testing.

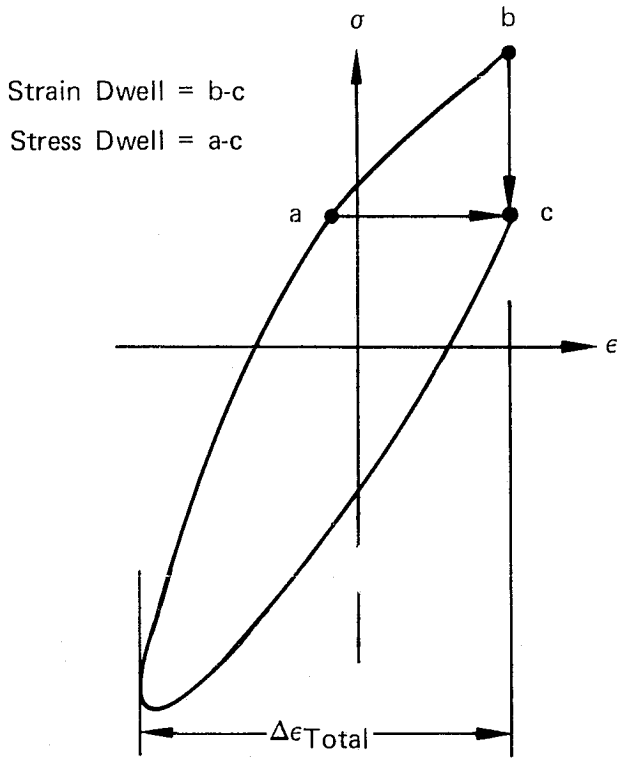

Figure 51. Comparison of Strain Dwell and Stress Dwell FD 95922

Section V.D.2.a described the computational and judgmental procedure used in predicting cyclic life under thermal-mechanical test conditions. Although successful, the prediction methodology presented has two serious shortcomings:

1. The same value for predicted life was selected for both in-phase and out-of-phase tests, even though it was felt beforehand, and subsequently verified (Section V.D.3.b), that a significant difference in life would be observed.

2. The effects of mean stress observed between tests TM-3 and TM-6, and between TM-2 and TM-5 are unaccountable with the present system. TM-3 and TM-6 differed only in test frequency, 2 cpm and 0.5 cpm, yet displayed mean loads of +2.89 kN (+650 lb_f) and +3.11 kN (+700 lb_f), respectively, a 0.22 kN (50 lb_f) increase in mean tensile load. Similarly, tests TM-2 and TM-5 exhibited mean loads of -3.78 kN (-850 lb_f) and -3.56 kN (-800 lb_f), or a 0.22 kN (50 lb_f) decrease in mean compressive load, due only to the difference in test frequency, 2 cpm and 0.5 cpm.

An investigation comparing the effects of strain and stress dwells, and considering the influence of non-zero mean strain would be useful additions to SRP technology.